An integrated model of energy-efficient timetabling of the urban rail transit system with multiple interconnected lines

Transportation Research Part C 129 (2021) 103171

Contents lists available at ScienceDirect

Transportation Research Part C

journal homepage: www.elsevier.com/locate/trc

An integrated model of energy-efficient timetabling of the urban rail transit system with multiple interconnected lines

Kang Huang [a,b,c], Feixiong Liao [b,*], Ziyou Gao [c,*]

[a] State Key Laboratory of Rail Traffic Control and Safety, Beijing Jiaotong University, Beijing, China
[b] Urban Planning and Transportation Group, Eindhoven University of Technology, Eindhoven, the Netherlands
[c] Key Laboratory of Transport Industry of Big Data Application Technologies for Comprehensive Transport, Ministry of Transport, Beijing Jiaotong University, Beijing, China

ARTICLE INFO

Keywords:
Urban rail transit
Energy-efficient timetabling
Bi-level model
User equilibrium

ABSTRACT

Urban rail transit (URT) has been considered an effective means of addressing urban congestion problems in metropolises. The operations of a URT system involve high energy consumption and its trade-off with passenger travel times. Existing energy-efficient timetabling studies have predominately focused on single URT lines and thus are incapable of accurately modeling the energy consumption in a URT network with transfer opportunities and synchronization between the URT lines. To extend the energy-efficient timetabling from one single line to multiple interlinked lines, we propose a bi-level model incorporating the operator's decision on a regular timetable and passengers' path choice in a URT network. The objective of energy consumption and timetable constraints of the upper level are linearized and formulated as mixed-integer linear programming. The lower level captures the user equilibrium based path choice behavior responding to the timetable. We develop a heuristic algorithm for the bi-level model that produces near-optimal timetable solutions in a relaxation process. The proposed model and solution algorithm are validated in the URT network of Xi'an (China). It is found that the energy consumption is considerably reduced, compared with using the current timetable, at the expense of an acceptable increase in the average travel time.

1. Introduction

Urban rail transit (URT), due to the low fare, high capacity, punctuality, and environmental friendliness, has attracted much attention in urban mobility in large cities (Yang et al., 2020). However, even though the URT is much more energy-efficient than other main transport modes for serving the same population (González-Gil et al., 2013, 2014), the URT faces a challenge in energy-saving. For instance, it is estimated that the Beijing URT will approximately use two billion kWh in 2020 (the same amount may supply a city with a population of 500 thousand for one year) and be the largest consumer of all single organizations in Beijing, which cause concerns to the local government and environment agencies (Lv et al., 2019). In the existing research, there are two research lines dedicated to energy efficiency in a URT system (Huang et al., 2019), namely, optimal train control and energy-efficient timetabling. Focusing on a single train on a track between two stations, the optimal train control aims at finding the optimal driving strategies in terms of speed profiles to minimize energy consumption (Howlett, 1996, 2000; Howlett and Pudney, 1998; Albrecht et al., 2013;

* Corresponding authors.
E-mail addresses: f.liao@tue.nl (F. Liao), zygao@bjtu.edu.cn (Z. Gao).

https://doi.org/10.1016/j.trc.2021.103171
Received 11 December 2020; Received in revised form 15 April 2021; Accepted 18 April 2021
Available online 8 June 2021

Table 1
Main differences between the present study and the existing ones in energy-efficient timetabling.

Reference	Scope	Passenger assignment	Model type	Solution method
Chevrier et al. (2013)	S	No	NP	GA
Li and Lo, (2014a, b)	S	No	NP	GA
Yang et al. (2015, 2016, 2017)	S	No	NP	GA
Gupta et al. (2016)	S	No	NP	N/A
Wang and Goverde, (2016, 2017, 2019)	S	No	NP	Heuristic policy
Yin et al. (2016)	S	No	MIQP	Approximate dynamic programming
Canca and Zarzo, (2017)	S	No	MILP	Gurobi
Yin et al. (2017)	S	Yes	MILP	Lagrangian relaxation-based heuristic algorithm
Liu et al. (2018)	S	No	NP	GA
Lv et al. (2019)	S	Yes	MILP	Gurobi
Su et al. (2019)	S	No	NP	Dynamic Programming and PSO
Yang et al. (2020)	S	Yes	NP	NSGA-II
This study	M	Yes	Bi-level MILP	Gurobi, a domain-knowledge based heuristic, and MSA

(S = Single line; M = Multiple lines; NP: Non-linear programming; MIQP: Mixed-integer quadratic programming; NSGA-II: Non-Dominated Sorting Genetic Algorithm II; N/A: Not available).

Scheepmaker et al., 2017). On the other hand, energy-efficient timetabling (Li and Lo, 2014a, b; Yang et al., 2015, 2016, 2017; Yin et al., 2016; Wang and Goverde, 2016, 2017) typically concerns the running time allocations of a fleet of trains on a URT line. As energy-efficient timetabling is the focus of attention, we review the most relevant studies in two research lines, i.e., (1) optimal train control for reducing energy consumption and (2) energy-efficient timetabling for single metro lines.

Optimal train control is a traditional problem based on the optimal control theory, in particular on the Pontryagin's Maximum Principle (PMP) (Albrecht et al., 2016a,b). The mathematical problem was conducted and applied under the control theory in the early years (Howlett and Pudney, 1995; Khmelnitsky, 2000; Liu and Golovitcher, 2003; Lai et al., 2020). The train control and speed profile include three sub-processes, namely, maximum acceleration, coasting, and maximum braking (Howlett and Pudney, 1998). The switching points of these sub-processes are at the core of train control. Howlett et al. (2009) showed that the optimal switching points for a steep section can be found by minimizing an intrinsic local energy function. Yang et al. (2018) analyzed the switching points and converted the relationship between running time and energy consumption into a strictly convex quadratic programming problem. To assist train drivers with optimal controls in real-time, some train on-board systems incorporated specific speed advice and train delays in operations (Panou et al., 2013). With the mass data generated in real operations and development of artificial intelligence, Huang et al. (2019) and Yin et al. (2020) applied machine learning methods, for example, random forest regression (RFR), support vector machine regression (SVR), and deep neural network (DNN), to optimize speed profiles.

Energy-efficient timetabling has recently been a hotspot topic (Li and Lo, 2014a, b; Zhao et al., 2015; Gupta et al., 2016; Ye and Liu, 2016; Yin et al., 2016, 2017; Canca and Zarzo, 2017; Yang et al., 2019; Mo et al., 2019a,b; Liu et al., 2020; Qu et al., 2020) in the study of energy efficiency of URT systems. For example, Li and Lo (2014a) considered the speed control and headway of a timetable by synchronizing train acceleration and braking to maximize the utilization of regenerative energy. It was later found by Li and Lo (2014b) that adjusting the cycle time of the URT line could further reduce energy consumption. These two studies formulated the problems in a non-linear system and applied a genetic algorithm (GA) to find the solutions. Considering uncertain dwell times, Yang et al. (2017) proposed an ε-constraint method in the GA framework to find Pareto optimal solutions to minimize the total energy consumption and passenger travel time. Utilizing passenger smart-card data as input for passenger demand, Yang et al. (2019) formulated a convex quadratic programming problem and developed an optimization-based approach to generate a timetable with stop-skipping patterns. By transferring arrival and departure times to time window constraints and relaxing the given timetable, Wang and Goverde (2019) proposed a multi-train trajectory optimization method with a base objective of minimizing multi-train energy consumption and an additional objective of eliminating conflicts between trains. Mo et al. (2019a) presented a bi-objective model to minimize energy consumption and passenger waiting time simultaneously, considering different train capacity constraints. A modified tabu search algorithm with a prior enumeration process was used to find near-optimal solutions. A few factors in a URT network affect the total energy consumption, e.g., rolling stocks and line lengths. Specifically, different lines in a URT network usually operate with different rolling stocks (Zhong et al., 2019), which affects train deadhead mileage, passenger flow, and energy consumption on the sections (Zhong et al., 2020). Mo et al. (2019b) integrated the optimal train timetable and rolling stock plan that optimized the brake-traction overlapping time at stations. Based on energy-regenerative technologies, Yang et al. (2020) formulated an optimization model considering energy allocation and passenger assignment to maximize regenerative energy utilization and minimize passenger travel time. A solution algorithm based on the Non-Dominated Sorting Genetic Algorithm II (NSGA-II) was developed to find the Pareto frontier. All of the above studies reported significant energy reductions of the newly generated timetables over the used timetables.

It is commonly known that the timetabling for a single URT line is an NP-hard problem (Cai and Goh, 1994). The timetabling problem becomes harder when energy-efficiency is incorporated. As summarized in Table 1, with the assumption of fixed passenger arrival rates and the absence of path choices, a few studies (e.g., Yin et al., 2017) suggested mixed-integer linear programming (MILP) formulations for single URT lines of less than 20 stations. With a similar assumption, some studies (e.g., Yang et al., 2020) considered non-linear formations and applied metaheuristic solution algorithms (e.g., GA and PSO). The energy-efficiency timetabling problem is even harder when considering passenger path choices in a URT network of multiple interconnected lines, which is probably the reason why no research of this kind has been done.

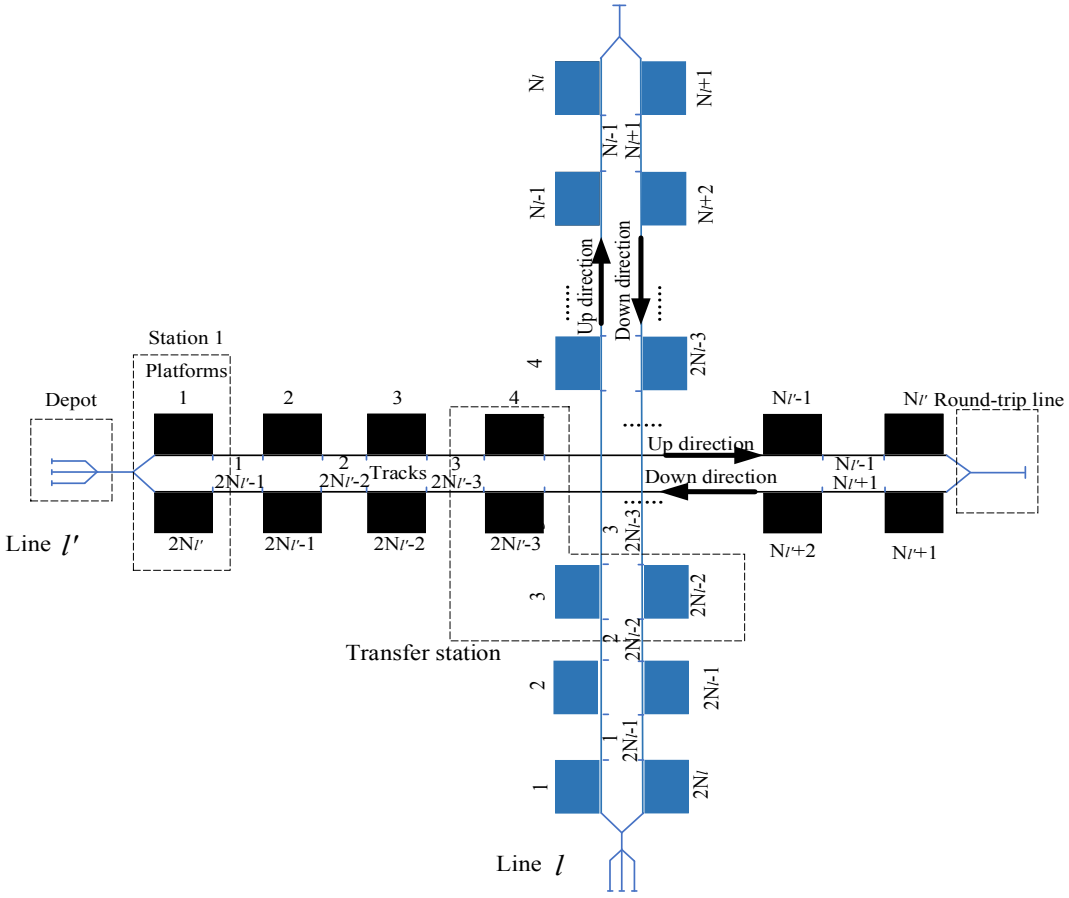

Fig. 1. An illustration of a URT network with two bidirectional lines.

Despite increasing research entries on energy-efficient timetabling, to the best of our knowledge, existing studies have been unexceptionally limited to single URT lines. This treatment is valid in a URT system with only one URT line or independent URT lines, which however does not hold in most modern URT systems. Although the power supply for each URT line is separated, the URT lines are associated with each other by passenger transfers and timetable synchronization among the URT lines. The modeling limitations cannot capture the accurate passenger allocation in the URT network and tend to produce unwanted chain effects on the calculation of energy consumption. Many studies have addressed the traditional timetabling problems of a URT network with multiple lines (e.g., Wong et al., 2008; Guo et al., 2018; Shang et al., 2018; Sun et al., 2018; Chen et al., 2019; Yao et al., 2019; Guo et al., 2020; Boroun et al., 2020; Huang et al., 2021), but none of them takes energy-efficiency into consideration.

Therefore, this study aims to extend the energy-efficient timetabling from a single line to multiple lines in a URT network. We propose a bi-level model framework considering timetabling and passenger path choices (including transfer choices) as an interactive process. The upper level model determines the optimal timetable and speed profiles under the given passenger path choices. The lower level model concerns passenger path choices by the receiving timetable from the upper level. Technically, we formulate the upper level optimization problem as mixed-integer linear programming (MILP). The lower level adopts a passenger assignment in a space–time network and is assumed that passengers adapt path choices until a user equilibrium (UE) state is reached.

To highlight the contributions of this study, we summarize the differences between this study and a few relevant studies in terms of modeling aspects in Table 1. First of all, our study is the first one extending the energy-efficient timetabling from a single line to multiple lines in a URT network. Second, although passenger assignment has recently been considered in energy-efficient timetabling (e.g., Su et al., 2019; Yang et al., 2020), these studies applied a one-off allocation based on simple heuristics of proportional assignment. This study considers more realistic UE-based feedback of passengers to the timetable. Third, most studies formulated one level of (non–)linear programming and applied (meta-)heuristic methods (e.g., GA and PSO), which might result in non-justifiable and non-reproducible solutions. In this study, we propose a bi-level model framework and develop a domain-knowledge based heuristic algorithm to obtain near-optimal solutions.

The remainder of this paper is organized as follows. Section 2 provides the problem description and modeling assumptions. Section 3 entails the modeling of synchronous URT lines and their interactions with passenger path choices in a bi-level model framework. Section 4 discusses the solution algorithm to the bi-level model. Section 5 presents a comprehensive case study in the URT system in the city of Xi'an (China) to verify the model and algorithm. Finally, Section 6 concludes the main contributions and provides suggestions

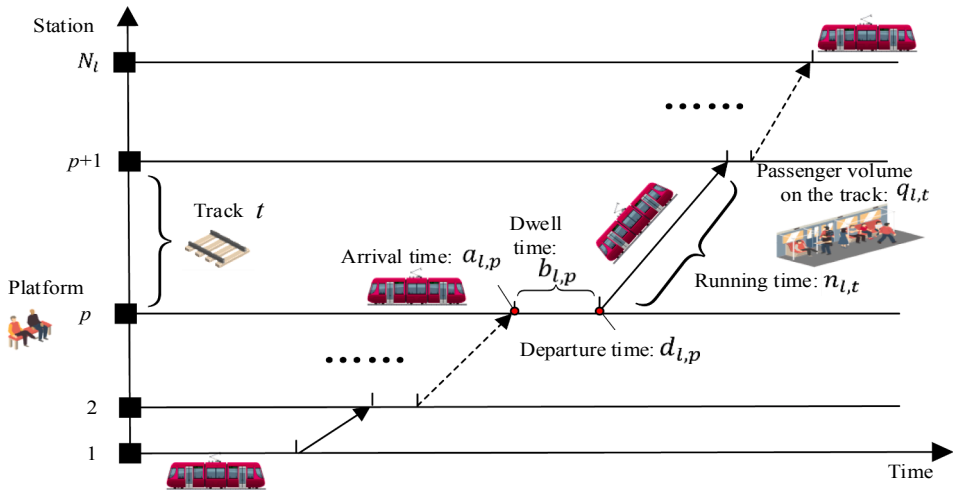

Fig. 2. Key variables for energy-efficient timetabling.

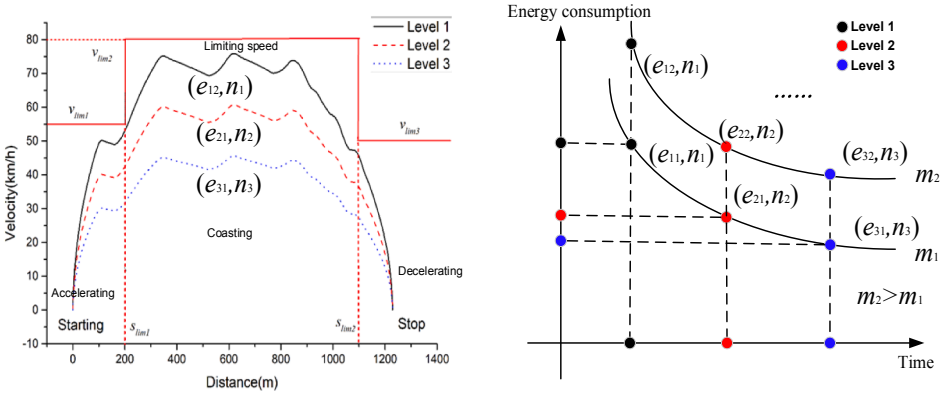

(a) Alternative speed profiles. (b) Energy consumption.

Fig. 3. Speed profiles at different levels and energy consumption with different weights.

for future research.

2. Problem description

The energy-efficient timetabling determines the elements of a timetable (e.g., arrival time, running time, departure time for each platform) with the minimum energy consumption while completing the tasks of transporting passengers. The passengers in the URT network may have multiple alternative paths. Therefore, passenger path choices should be taken into consideration. In Fig. 1, we use a typical and simplest URT network with two crossed lines to illustrate the timetabling problem. Suppose there are N_l and $N_{l'}$ stations, $2N_l$ and $2N_{l'}$ platforms, and $2N_l-2$ and $2N_{l'}-2$ tracks (one track between two neighboring platforms) on line l and l', respectively. The platforms and tracks are arranged and numbered in order. A train departing from platform 1 to platform N_l is in the up-direction, while departing from the platform N_l+1 to platform $2N_l$ is in the down-direction. There are four platforms on the transfer station, i.e., platform 4 and $2N_{l'}-3$ of line l', platform 3 and $2N_{l'}-2$ of line l. Based on this layout, key components for energy-efficient timetabling are represented in Fig. 2. A passenger starts from its origin platform and goes through a series of activities (waiting, boarding, and alighting) to reach the destination platform.

For illustration, as shown in Fig. 3(a), the running process on each track has a set of alternative discrete speed profiles and each profile has three main stages (accelerating, coasting, and decelerating) with speed limitations for different geographical conditions. Commonly, the speeds and running times are dynamic according to the operation level of the on-board control systems called ATO (Automatic Train Operation). The drivers intervene and control the trains only in case of emergencies (Yin et al., 2017; Mo et al., 2019a). Based on the train control theory, the energy consumption on track t is a non-linear function of the loading weight ($m_{l,t}$) and running time $n_{l,t}$, denoted by $e(m_{l,t}, n_{l,t})$. For each track, one level of on-board operation corresponds to one speed profile and thus one specific running time. A higher operation level usually corresponds to a lower speed. Denote the running time at operation level g on track t of line l by $n_{l,t,g}$. For simplicity, $n_{l,t,g}$ is simplified as n_g given a track. To illustrate the relationships, suppose that operation level g is associated with running times n_g. Given train loading weight level m, the energy consumption e_{gm} (for the sake of notational

simplicity) has the following features. As shown in Fig. 3(b), for the same loading, a higher speed profile needs more energy consumption for acceleration and coasting (the main stages of energy consumption). Therefore, running times and energy consumption satisfy $n_1 \leq n_2 \leq n_3$ and $e_{11} \geq e_{21} \geq e_{31}$ respectively. For the same operation level, the heavier the train is, the more energy consumption is involved (i.e., $e_{12} \geq e_{11}; e_{22} \geq e_{21}; e_{32} \geq e_{31}$).

Overall, operation level g and train loading $m_{l,t}$ determine the running time and energy consumption given operation conditions (train type and ATO system). The train loading, $m_{l,t}$, depends on the passenger volume on the train. Therefore, there are two types of decision variables, i.e., timetable and passenger distribution on the network, in the energy-efficient timetabling problem for multiple lines. The notations are defined below.

2.1. Assumptions

The following assumptions are made to facilitate the development of the model framework.

Assumption 1. The trains are scheduled periodically (e.g., during peak hours) and all passengers can board the train in a planning period. Periodic timetables are widely adopted by URT operators using the space–time network modeling method (Shang et al., 2018, Zhang et al., 2019).

Assumption 2. In the URT network, the transfer time consists of walking time and waiting time, where the walking time is fixed given the transfer station and the waiting time is related to the headway of the URT line.

Assumption 3. To accommodate all passengers, the passenger arrival rate determines the headway for a periodic timetable. The time-dependent passenger arrival rate at a platform is fixed as the average during the planning period.

Assumption 4. Given a timetable, the passengers in the URT network adapt path choice to reach a UE state by long-term day-to-day adjustments (Bie and Lo, 2010; Djavadian and Chow, 2017).

Assumption 5. The URT operator pursues the minimum energy consumption, while the passengers seek the least generalized travel cost.

2.2. Notations

The following parameters, sets, intermediate variables, and decision variables are used in the model.
Parameters:

Γ	the length of the planning period
γ_l	train capacity of line l
N_l	number of stations on line l
m_l^0	weight of empty train on line l
κ^w	cost coefficient of waiting time
κ^r	cost coefficient for crowding of in-vehicle time
κ^t	cost coefficient of transfer time

Elements and sets:

l, L	index of line and set of lines
t, T_l	index of track and set of tracks on line l
p, P_l	index of platform and set of platforms on line l
H_l	set of headways on line l
Ω_l	set of frequencies on line l
N_l	number of stations on line l
$[h^{\mathrm{O}}, h^{\mathrm{E}}]$	time range of the feasible headway
$[b^{\mathrm{O}}, b^{\mathrm{E}}]$	time range of the feasible dwell time
j, J	index of OD (origin–destination) pair and set of the OD pairs
i, I	index of arc and set of arcs
r, R_j	index of path and path belongs to OD pair j

Intermediate variables related to the timetable and passenger assignment:

$\widehat{v}_{l,p}^{+}, \widehat{v}_{l,p}^{-}$	average number of boarding/alighting passengers at platform p on line l
$v_{l,p}^{+}, v_{l,p}^{-}$	boarding/alighting passengers at platform p on line l
$y_{l,p}^{+}, y_{l,p}^{-}$	Boarding/alighting time at platform p on line l
$\delta_{l,k}$	0–1 variable with $\sum_{l,k}\delta_{l,k} = 1$
e_l	energy consumption of line l
Q_j	passenger volume of OD pair j
u_{ijr}	0–1 variable, $u_{ijr} = 1$ if arc i belongs to path r of OD pair j; otherwise, $u_{ijr} = 0$
$\beta_i^{l,t}$	0–1 variable, $\beta_i^{l,t} = 1$ if arc i corresponds to track t on line l ; otherwise, $\beta_i^{l,t} = 0$
$q_{l,t}$	passenger volume on track t of line l
$q_l^{\max}$	the maximum number of passengers on the tracks of line l
q_i	the passenger volume on running arc i
z_j^r	cost of path r that belongs to OD pair j
μ_j	the minimum cost of od pair j at the user equilibrium state

Decision variables related to the timetable and passenger assignment:

$a_{l,p}$	arrival time of the first train at platform p on line l
$b_{l,p}$	dwell time of the first train at platform p on line l
Φ_l	cycle time of line l
$d_{l,p}$	departure time of the first train at platform p on line l
$n_{l,t}$	running time of the first train on track t of line l
f_l	frequency of line l
h_l	headway of line l
φ_l	fleet size of line l
x_i	passenger flow on arc i
q_j^r	passenger flow assigned to path r of OD pair j

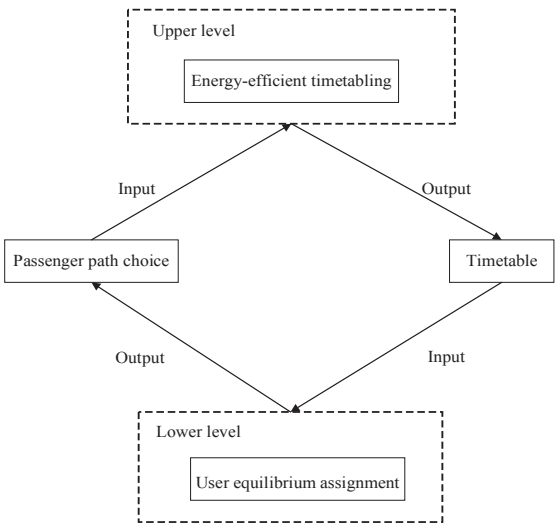

Fig. 4. Integrated model framework for the energy-efficient timetabling in a URT network.

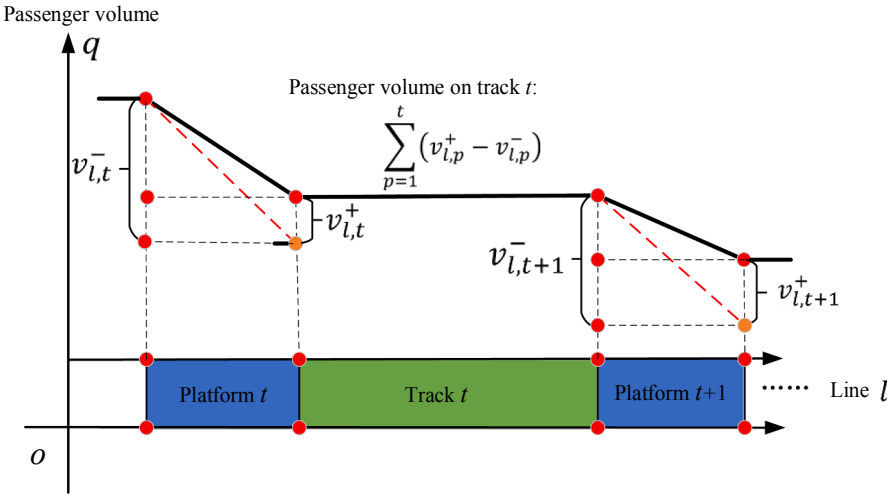

Fig. 5. Passenger volume on track t.

3. Model

The primary difference between single-line and multiple-lines is whether the transfer is allowed. Passenger path choices are the most salient differences between a single line and multiple lines in a URT network. Although the power supply for each URT line is separated, the URT lines are associated with each other by passenger transfers and synchronization between the URT lines. For a URT network with transfer opportunities, passenger transfer and path choice should be incorporated in the energy-efficient timetabling. Passengers' path choice and the operator's timetable have a typical game relationship (Assumption 5). Therefore, we propose a bi-level model for the energy-efficient timetabling in a URT network to model the interactions. The energy-efficient timetabling model at the upper level is formulated as mixed-integer linear programming. The lower level is specified as a UE-based passenger assignment in the URT network. Fig. 4 shows the bi-level model framework, in which the upper level is an energy-efficient timetabling model that needs the input of passenger path choices, and the lower level is the passenger assignment responding to a timetable. The bi-level optimization framework divides the decision variables into two parts, i.e., timetable and passenger flow patterns in the URT network. Since it is not straightforward to formulate the lower-level user equilibrium conditions as constraints in the upper-level model, the timetabling (up-level) and passenger flow assignment (lower-level) are carried out in a heuristic relaxation process to seek quality timetable solutions.

3.1. Energy-efficient timetabling model (Upper level)

Focusing on transfer between multiple lines, we optimize a periodic timetable with a fixed headway of each line at the upper level. In the following two subsections, we first propose the energy-efficient timetabling in non-linear formulations to minimize the total energy consumption. Then, the model is transformed into MILP by linearizing the non-linear objective and constraints.

3.1.1. Energy-efficient timetabling model in non-linear formulation

The timetable-related constraints and objective of energy consumption are presented as follows. As the designed timetable is periodic and parallel, the time schedules of the first train are repeated cyclically by the ensuing trains on the same URT line. For track t on line l, $\forall t \in T_l, \forall l \in L$, the definitional relationship among departure time ($d_{l,t}$), running time ($n_{l,t}$) and arrival time ($a_{l,t+1}$) is formulated as Eq. (1). For the dwell time on platform p ($\forall p \in P_l$) on line l, the relationship between departure time ($d_{l,p}$) and arrival time ($a_{l,p}$) is formulated as Eq. (2). To allow enough time for alighting and boarding and avoid waiting long at the platform, there is a time range, $[b^{O}, b^{E}]$, of the feasible dwell time $b_{l,p}$ in Eq. (3). There is also a time range $[h^{O}, h^{E}]$ in Eq. (4) for the feasible train headway h_l. The minimum headway is determined by the signaling system for safety considerations and the maximum value is usually related to the service level. The departure frequency f_l determines the train fleet size during the planning period and is associated with the headway by Eq. (5). To ensure frequency f_l is an integer, h_l is specified as a divisor of 3600 (considering one hour as the time frame). As Canca and Zarzo, (2017) suggested, there are alternative headway values, for instance, 120, 180, 240, 300, 360, 600, 720, 900, 1200, and 1800 in seconds. The cycle time Φ_l is the time expense by a train completing a loop in the bi-directional line, given as Eq. (6), where η_l denotes the turning-around time of line l.

$$a_{l,t+1} - d_{l,t} = n_{l,t}, \quad \forall l \in L, \forall t \in T_l \tag{1}$$

$$b_{l,p} = d_{l,p} - a_{l,p}, \quad \forall l \in L, \forall p \in P_l \tag{2}$$

$$b^{O} \le b_{l,p} \le b^{E}, \quad \forall l \in L, \forall p \in P_l \tag{3}$$

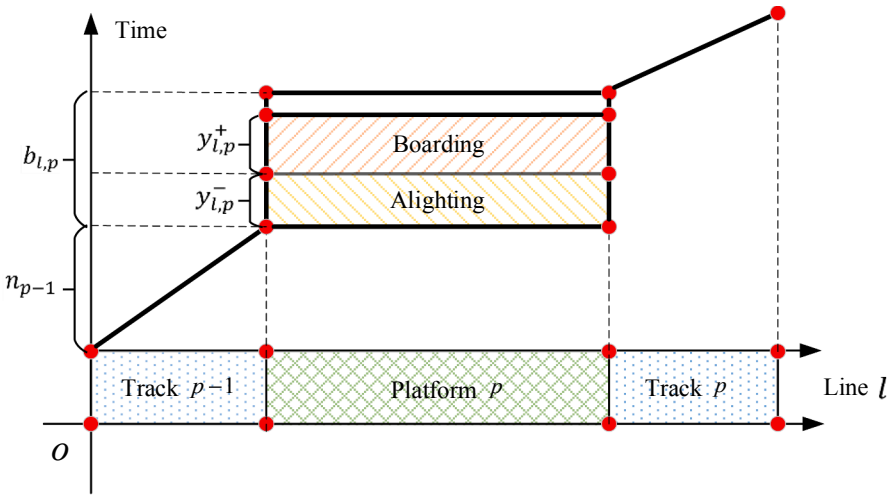

Fig. 6. Alighting and boarding constraints of dwell time.

$$h^{\mathrm{O}} \le h_l \le h^{\mathrm{E}}, \quad \forall l \in L \tag{4}$$

$$f_l \cdot h_l = 3600, \quad \forall l \in L \tag{5}$$

$$\Phi_l = 2 \cdot \eta_l + \sum_{t \in T_l} n_{l,t} + \sum_{p \in P_l} b_{l,p}, \quad \forall l \in L \tag{6}$$

The passenger volume on track t can be computed by the accumulations on the track, which is illustrated in Fig. 5. Starting from the first platform in one direction, $v^+_{l,p}$ and $v^-_{l,p}$ denote the numbers of boarding and alighting passengers at platform p of line l respectively. As shown in Eq. (7), the passenger volume on track t is $\sum_{p=1}^{t}\left(v^+_{l,p} - v^-_{l,p}\right)$ in the up-direction ($t < N$); likewise, the passenger volume is $\sum_{p=\mathrm{N}_l+1}^{t}\left(v^+_{l,p} - v^-_{l,p}\right)$ in the down-direction. The maximum number of passengers on the tracks of line l , $q_l^{\max}$ in Eq. (8), is an essential indicator for accommodating the passenger demand within the train capacity. According to Assumption 4, the average number of boarding passengers ($\widehat{v}^+_{l,p}$)and alighting passengers ($\widehat{v}^-_{l,p}$) (passengers per second) are given in Eq. (9). In addition, there are constraints on the numbers of boarding and alighting passengers during the dwelling process. ε^- and ε^+ denote the alighting and boarding rates (seconds per passenger) respectively, which are determined by the width and number of train doors. Then, the alighting time ($y^-_{l,p}$) and boarding time ($y^+_{l,p}$) at platform p can be computed in Eqs. (10)–(11).

$$q_{l,t} = \begin{cases} \sum_{p=1}^{t}\left(v^+_{l,p} - v^-_{l,p}\right), & \text{if } t \in [1, \mathrm{N}_l] \\ \sum_{p=\mathrm{N}_l+1}^{t}\left(v^+_{l,p} - v^-_{l,p}\right), & \text{if } t \in [\mathrm{N}_l + 1, 2\mathrm{N}_l] \end{cases} \tag{7}$$

$$q_l^{\max} = \max_t q_{l,t}, \quad \forall t \in T_l \tag{8}$$

$$\widehat{v}^+_{l,p} = \frac{v^+_{l,p}}{\Gamma}, \widehat{v}^-_{l,p} = \frac{v^-_{l,p}}{\Gamma}, \quad \forall l \in L, \forall p \in P_l \tag{9}$$

$$y^-_{l,p} = \widehat{v}^-_{l,p} \cdot h_l \cdot \varepsilon^-, \quad \forall l \in L, \forall p \in P_l \tag{10}$$

$$y^+_{l,p} = \widehat{v}^+_{l,p} \cdot h_l \cdot \varepsilon^+, \quad \forall l \in L, \forall p \in P_l \tag{11}$$

The dwell times need to be long enough to complete the alighting and boarding processes. As shown in Fig. 6, the alighting and boarding processes take time $\left(y^-_{l,p} + y^+_{l,p}\right)$. The dwell time should be no less than the alighting and boarding time, i.e., $b_{l,p} \ge \left(y^-_{l,p} + y^+_{l,p}\right)$, rearranged as (12). Since the opening and closing times of the train doors are short, they are not considered in the dwelling process.

$$b_{l,p} \ge h_l \cdot \left(\varepsilon^- \cdot \widehat{v}^-_{l,p} + \varepsilon^+ \cdot \widehat{v}^+_{l,p}\right), \quad \forall l \in L, \forall p \in P_l \tag{12}$$

The headway is associated with the fleet size φ_l, expressed as Eq. (13). By replacing headway h_l with $\frac{f_l}{3600}$, the fleet size is formulated

as Eq. (14). We can see that if cycle time $\Phi_l \geq 3600$s, then $\varphi_l \geq f_l$. If $\Phi_l < 3600$s (there may be URT lines with short cycles), then $\varphi_l < f_l$. Economically, the fleet size should not be greater than the maximum number of trains in Eq. (15). There is a corresponding capacity of each line, γ_l, for the consideration of limited room and passenger comfort. To accommodate all passenger demands given the capacity, frequency f_l should be large enough to satisfy the constraint as Eq. (16). Constraint (16) can be in another form due to $f_l \cdot h_l = 3600$ as Eq. (17). Therefore, if the train capacity is fixed after determining the train units, the maximum passenger volume in one hour is $\frac{3600 \cdot \gamma_l}{h^E}$. Additionally, with an increase in $q_l^{\max}$, the headway should be shorter. Given average passenger weight τ, the passenger load $m_{l,t}$ on track t is formulated as Eq. (18).

$$\varphi_l = \frac{\Phi_l}{h_l}, \quad \forall l \in L \tag{13}$$

$$\varphi_l = \Phi_l \cdot \frac{f_l}{3600}, \quad \forall l \in L \tag{14}$$

$$\varphi_l \leq \varphi_l^{\max}, \quad \forall l \in L \tag{15}$$

$$q_l^{\max} \leq \gamma_l \cdot f_l, \quad \forall l \in L \tag{16}$$

$$q_l^{\max} \cdot h_l \leq \gamma_l \cdot 3600, \quad \forall l \in L \tag{17}$$

$$m_{l,t} = \frac{q_{l,t} \cdot \tau}{f_l} = \frac{q_{l,t} \cdot \tau \cdot h_l}{3600}, \quad \forall l \in L, \forall t \in T_l \tag{18}$$

The objective of energy-efficient timetabling is the total energy consumption of the URT network. The energy consumption for line l is given as Eq. (19) and the total energy consumption of the URT network is given as Eq. (20).

$$e_l = f_l \cdot \sum_{t \in T_l} e\left(m_{l,t}, n_{l,t}\right), \quad \forall l \in L \tag{19}$$

$$E = \sum_{l \in L} e_l \tag{20}$$

where e_l is the energy consumption of line$l$ and E is the total energy consumption of the URT network.

As formulated in Eq. (20), the energy consumptions of the URT lines are independent of each other. However, the linkage between the URT lines are reflected in $q_{l,t}$ of Eq. (10) and $m_{l,t}$ of Eq. (19) during the course of passenger path choice. One derived feature is that Eq. (20) can be solved in parallel given the passenger path choices. This implicit decomposition of energy consumption reduces the complexity of energy-efficient timetabling.

3.1.2. *Energy-efficient timetabling model as MILP*

To make the energy-efficient timetabling problem tractable, we linearize the non-linear objective function (Eq. (20)) and two constraints (Eqs. (5) and (13)). First, the non-linear objective function is linearized by utilizing discrete speed levels. Then, based on alternative headways, the constraints are linearized by the Big M method and variable transformations.

Denote the basic energy consumption on track t at level g by $e_{l,t,g}^0$ when the train is empty with weight m_l^0. When the passengers are loaded on the train, the total weight is $m_l^0 + m_{l,t}$. Thus, the energy consumption in a neat form is equal to $\left(1 + \frac{m_{l,t}}{m_l^0}\right) e_{l,t,g}^0$ (the multiplication sign $\cdot$ is omitted for simplicity). The side-effect of this formulation on the energy consumption is negligible because the energy consumption is mainly determined by the mechanical running resistance and the kinetic energy (other parts, such as aerodynamical resistance and the ingoing air volume, are only in very small proportions).

Given a set of operation levels on track t of line l, G_{lt}, a set of binary variables $\theta_{l,t,g}$ is introduced: $\theta_{l,t,g} = 1$ if level g is selected; otherwise, $\theta_{l,t,g} = 0$. For track t, only one level can be selected, expressed as Eq. (21). Given the selected level, the running time on a track is fixed. Therefore, the running time for track t of line l can be formulated in Eq. (22).

$$\sum_{g \in G_{lt}} \theta_{l,t,g} = 1, \quad \forall l \in L, \forall t \in T_l \tag{21}$$

$$n_{l,t} = \sum_{g \in G_{lt}} \theta_{l,t,g} n_{l,t,g}, \quad \forall l \in L, \forall t \in T_l \tag{22}$$

Therefore, energy consumption $e\left(m_{l,t}, n_{l,t}\right)$ in Eq. (19) can be replaced by

$$e\left(m_{l,t}, n_{l,t}\right) = \sum_{g \in G_{l,t}} \theta_{l,t,g} \left(1 + \frac{m_{l,t}}{m_l^0}\right) e_{l,t,g}^0, \quad \forall l \in L, \forall t \in T_l \tag{23}$$

Eq. (23) consists of the product of binary variable $\theta_{l,t,g}$ and variable $\left(1+\frac{m_{l,t}}{m_l^0}\right)$. To linearize Eq. (23), we introduce a new set of variables $\rho_{l,t,g}$: $\rho_{l,t,g}=\left(1+\frac{m_{l,t}}{m_l^0}\right)$ if $\theta_{l,t,g}=1$; otherwise, $\rho_{l,t,g}=0$. Then, a set of constraints are introduced as

$$\begin{cases} \left(1+\frac{m_{l,t}}{m_l^0}\right)-\Lambda_1\left(1-\theta_{l,t,g}\right)\le\rho_{l,t,g}\le\left(1+\frac{m_{l,t}}{m_l^0}\right)+\Lambda_1\left(1-\theta_{l,t,g}\right) \\ \rho_{l,t,g}\le\theta_{l,t,g}\Lambda_1 \\ \rho_{l,t,g}\ge 0 \\ \forall l\in L, t\in T_l, g\in G_{lt} \end{cases} \tag{24}$$

where Λ_1 is an upper bound of $\rho_{l,t,g}$, for instance, $\max\left(1+\frac{m_{l,t}}{m_l^0}\right)e_{l,t,g}^0$. Therefore, $e\left(m_{l,t},r_{l,t}\right)$ can be replaced by $\sum_g\rho_{l,t,g}e_{l,t,g}^0,\forall g\in G_{lt}$.

Denote an element of H_l by $h_{l,k}\left(k\le|\Omega_l|\right)$ and an element of Ω_l by $f_{l,k}$. To keep $h_{l,k}f_{l,k}=3600$, $h_{l,k}$ is in ascending order if $f_{l,k}$ is given in descending order.

To linearize the constraints, we introduce a series of intermediate binary variables $\delta_{l,k}$. The sum of the binary variables $\delta_{l,k}$ is equal to 1 in Eq. (25). The binary variable $\delta_{l,k}$ and the element $h_{l,k}$ can be utilized to represent the headway as the sum of their product in Eq. (26). Similarly, the frequency can be expressed in Eq. (27). Recall that constraints (5) and (13) are non-linear. After introducing $\delta_{l,k}$, H_l, and Ω_l, constraint (5) is linearized. Constraint (13) can be rewritten as Eq. (28).

$$\sum_{k\le|\Omega_l|}\delta_{l,k}=1,\quad\forall l\in L \tag{25}$$

$$h_l=\sum_{k\le|\Omega_l|}\delta_{l,k}h_{l,k},\quad\forall l\in L \tag{26}$$

$$f_l=\sum_{k\le|\Omega_l|}\delta_{l,k}f_{l,k},\quad\forall l\in L \tag{27}$$

$$\Phi_l=\sum_{k\le|\Omega_l|}\delta_{l,k}h_{l,k}\varphi_l,\quad\forall l\in L \tag{28}$$

To linearize Eq. (28), a set of intermediate variables $\alpha_{l,k}$ is further introduced: $\alpha_{l,k}=\varphi_l$ if $\delta_{l,k}=1$; otherwise, $\alpha_{l,k}=0$. The linearization is achieved by a set of constraints in Eq. (29), where Λ_2 is an upper bound of $\alpha_{l,k}$, for example, $\Lambda_2=\max\varphi_l h_l,\forall l\in L$. The cycle time of line l is given in Eq. (30).

$$\begin{cases} \varphi_l-\Lambda_2\left(1-\delta_{l,k}\right)\le\alpha_{l,k}\le\varphi_l+\Lambda_2\left(1-\delta_{l,k}\right) \\ \alpha_{l,k}\le\delta_{l,k}\Lambda_2 \\ \alpha_{l,k}\ge 0 \\ \forall k\le|\Omega_l|,\forall l\in L \end{cases} \tag{29}$$

$$\Phi_l=\sum_{k\le|\Omega_l|}\alpha_{l,k}h_{l,k},\quad\forall l\in L \tag{30}$$

With the new variables, the objective is expressed as

$$e_l=\sum_{k\le|\Omega_l|}\left(\delta_{l,k}f_k\right)\sum_{t\in T_l}\sum_{g\in G_{lt}}\left(\rho_{l,t,g}e_{l,t,g}^0\right)=\sum_{k\le|\Omega_l|}\sum_{t\in T_l}\sum_{g\in G_{lt}}\left(\rho_{l,t,g}e_{l,t,g}^0\delta_{l,k}f_k\right)=\sum_{k\le|\Omega_l|}\sum_{t\in T_l}\sum_{g\in G_{lt}}\left(\rho_{l,t,g}\delta_{l,k}\right)\left(e_{l,t,g}^0f_k\right) \tag{31}$$

Furtherly, we replace $(\rho_{l,t,g}\delta_{l,k})$ by a new variable $\lambda_{l,t,g,k}$, where $\lambda_{l,t,g,k}=\rho_{l,t,g}$ when $\delta_{l,k}=1$ and $\lambda_{l,t,g,k}=0$ when $\delta_{l,k}=0$. The relationship between $\lambda_{l,t,g,k}$, $\rho_{l,t,g}$, and $\delta_{l,k}$ are described by constraints (32), where Λ_3 is the upper bound of $\lambda_{l,t,g,k}$, for instance, $\max\left(1+\frac{m_{l,t}}{m_l^0}\right)e_{l,t,g}^0f_k,\forall l\in L,\forall t\in T_l,g\in G_{l,t},k\le|\Omega_l|$. Taken together, the linear formulation of the objective is shown as Eq. (33).

$$\begin{cases} \rho_{l,t,g}-\Lambda_3\left(1-\delta_{l,k}\right)\le\lambda_{l,t,g,k}\le\rho_{l,t,g}+\Lambda_3\left(1-\delta_{l,k}\right) \\ \lambda_{l,t,g,k}\le\delta_{l,k}\Lambda_3 \\ \lambda_{l,t,g,k}\ge 0 \\ \forall l\in L, t\in T_l, g\in G_{lt}, k\le|\Omega_l| \end{cases} \tag{32}$$

Table 2
Numbers of variables and constraints in the UL.

Variables or constraints	Numbers in the UL
Arrival time, $a_{l,p}$; dwell time, $b_{l,p}$; departure time, $d_{l,p}$	$\sum_{l\in L}\lvert P_l\rvert$
Running time, $n_{l,t}$; loading weight, $m_{l,t}$	$\sum_{l\in L}\lvert T_l\rvert$
Frequency, f_l; headway, h_l; fleet size, φ_l; cycle time, Φ_l	$\lvert L\rvert$
Intermediate binary variable, $\delta_{l,k}$	$\sum_{l\in L}\lvert\Omega_l\rvert$
Intermediate continuous variable, $\rho_{l,t,g}$	$\sum_{l\in L}\sum_{t\in T_l}\lvert G_{lt}\rvert$
Intermediate continuous variable, $\lambda_{l,t,g,k}$	$\sum_{l\in L}\sum_{t\in T_l}\lvert G_{lt}\rvert\lvert\Omega_l\rvert$
Constraints (1), (7), (9)–(12), (18), (22)	$\sum_{l\in L}\lvert T_l\rvert$
Constraints (2)–(3)	$\sum_{l\in L}\lvert P_l\rvert$
Constraints (4), (6), (8), (17), (26)–(27), (30)	$\lvert L\rvert$
Constraints (21)	$\sum_{l\in L}\lvert\Omega_l\rvert$
Constraints (24)	$3\sum_{l\in L}\sum_{t\in T_l}\lvert G_{lt}\rvert$
Constraints (29)	$3\sum_{l\in L}\lvert\Omega_l\rvert$
Constraints (32)	$3\sum_{l\in L}\sum_{t\in T_l}\lvert G_{lt}\rvert\lvert\Omega_l\rvert$

$$E=\sum_{l\in L}\sum_{t\in T_l}\sum_{g\in G_{lt}}\sum_{k\le|\Omega_l|}\lambda_{l,t,g,k} \tag{33}$$

With the objective and constraints linearized, the upper level model (UL for short) is transformed into a MILP formulation as

$$\text{UL}:\min E=\sum_{l\in L}\sum_{t\in T_l}\sum_{g\in G_{lt}}\sum_{k\le|\Omega_l|}\lambda_{l,t,g,k}$$

s.t. Eqs. (1)–(4), (5)–(12), (15), (17)–(18), (21)–(22), (24)–(27), (29)–(30), (32)

As the UL is in mixed-integer linear formulations, we can obtain the exact energy-efficient timetable solution by optimization solvers (e.g., Cplex and Gurobi) given the passenger path choices. It is noteworthy that the linearization of the constraints by the Big M method and variable transformation does not modify the space of feasible solutions. In the UL, the total number of variables is the sum of those in each line. The detailed numbers of variables and constraints are listed in Table 2 to reflect the true complexity of the model. The total number of variables is $4|L|+3\sum_l|P_l|+2\sum_l|T_l|+\sum_l|\Omega_l|+\sum_l\sum_t|G_{lt}|+\sum_l\sum_t|G_{lt}||\Omega_l|$, where operator $|\cdot|$ gives the cardinality of a set. The total number of constraints is $7|L|+2\sum_l|P_l|+8\sum_l|T_l|+4\sum_l|\Omega_l|+3\sum_l\sum_t|G_{lt}|+3\sum_l\sum_t|G_{lt}||\Omega_l|$. The numbers of variables and constraints for line l are $3|P_l|+2|T_l|+|\Omega_l|+\sum_t|G_{lt}|+\sum_t|G_{lt}||\Omega_l|$ and $2|P_l|+8|T_l|+4|\Omega_l|+3\sum_t|G_{lt}|+3\sum_t|G_{lt}||\Omega_l|$, $\forall t\in T_l$, respectively. Due to the implicit decomposition, the URT line with the most variables and constraints dictates the complexity of the UL, which is under the capacity of the optimization solvers.

3.2. Passenger assignment (Lower level)

Passenger path choice is the key to URT operations. Much research has been done on passenger path choice in traffic networks. The majority of studies revolve around the UE-based traffic assignment (Wardrop, 1952; Nguyen and Pallottino, 1988; Spiess and Florian, 1989; Wu et al., 1994; Nuzzolo et al., 2001; Gentile et al., 2005; Jiang and Szeto, 2016; Shang et al., 2019,). However, little research has been thus far dedicated to passenger assignment for energy-efficient timetabling in a URT network. We formulate a passenger assignment model in a one-time instance of the space–time URT network as the lower level (LL for short) of the bi-level model.

We first construct the space–time URT network responding to a timetable generated from the UL model. In the space–time URT network, crowding, waiting, and transfers should be considered for defining passenger travel cost (disutility) on the paths. Given a timetable, the passenger flow patterns influence crowding on different running arcs. In line with the literature of path choice in traffic networks, we assume that the passengers adjust path choices to reach a user equilibrium (UE) state, at which all selected paths have an equal and minimum cost (Assumption 4). The space–time network consists of

five types of arcs (virtual arc, waiting arc, running arc, transfer arc, and arrival arc) and two types of nodes (physical node for the platform and virtual node for the station). One station is extended into one virtual node and two real nodes corresponding to the two platforms. The virtual arc connects the platforms of the same station. The waiting arc represents the waiting stage before boarding at the origin station of a trip. Running arcs represent physical movements over the tracks. A transfer arc bridges the platforms of the feeder line and the platforms of the connecting line at the transfer station. The arrival arc refers to the final stage of a trip leaving the destination platform. One temporal instance of the space–time network is illustrated in Fig. 7. For passengers departing from origin node o to destination node d, they first traverse the waiting arc to take the train on the running arc; after that, they arrive at the transfer station and go through the transfer arc to the connecting line. Next, they take running arcs again and finally reach the destination. Since we focus on a periodic timetable (Assumption 1), the space–time network has a common backbone structure. The generalized costs of the different arcs are defined below.

The cost of the virtual arc i, $c_i(i\in I^v)$, is considered zero in Eq. (34). Similarly, the cost of the arrival arc $c_i(i\in I^a)$ is also considered zero.

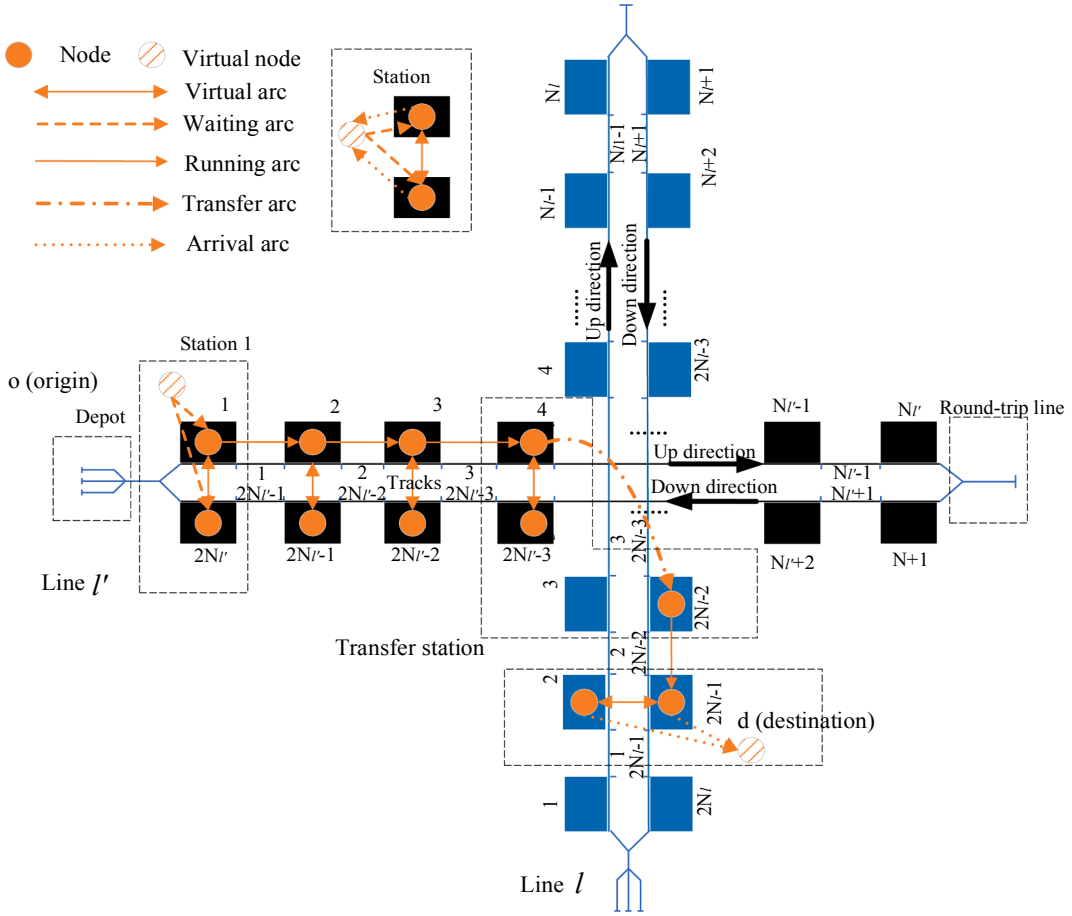

Fig. 7. An illustration of the expanded network.

$$c_i = 0, i \in I^v \cup I^a \tag{34}$$

where I^v and I^a are the sets of virtual arcs and arrival arcs respectively.

According to Assumption 4, the time-dependent passenger arrival rate at a platform is fixed as the

average during the planning period. The average waiting time at a platform is considered half of the headway (Ceder and Tal, 2001). Thus, the cost of a waiting arc is simply set as

$$c_i = \kappa^w \left(\frac{h_l}{2}\right), \quad i \in I^w \tag{35}$$

where κ^w is the cost coefficient of waiting time and I^w is the set of waiting arcs.

In the literature of route choice in a public transport system, crowding is often considered an important factor affecting passenger route choice (Liu et al., 2016; Fu and Lam, 2018). In this study, the passenger crowding effect is considered on the running arcs of the URT network. The crowding is directly determined by the passenger volume. Note that the crowding in URT is different from the crowding on the road surfaces. Crowding on the roads is out-the-vehicle which causes losses of time, but crowding in URT is in-vehicle which causes discomfort other than losses of time. Therefore, the cost of a running arc is determined by the running time of each track and the crowding effect (Chen et al., 2015), formulated in a BPR-like (Bureau of Public Road) form as

$$c_i = \left(1 + \frac{\kappa^r \cdot q_{l,t}}{f_l \cdot \gamma_l}\right) n_{l,t}, \quad i \in I^r \tag{36}$$

where κ^r is the crowding coefficient of in-vehicle time and I^r is the set of running arcs.

According to Assumption 2 and Eq. (36), the cost of a transfer arc is given as

$$c_i = \kappa^t \left(w_i + \frac{h_i}{2}\right), \quad i \in I^t \tag{37}$$

where κ^t is cost coefficient of transfer time, w_i is the fixed walking time for transfer arc i at a specific station, h_i is the headway of the connecting line on transfer arc i, and I^t is the set of transfer arcs.

Based on the generalized arc costs in the space–time URT network, the generalized path cost for an OD pair is formulated in an additive form as Eq. (38). The UE condition is given in Eq. (39).

$$z_j^r = \sum_i c_i \cdot u_{ijr}, \quad \forall i \in I \tag{38}$$

$$\mu_j - z_j^r \begin{cases} = 0, q_j^r > 0 \\ \leq 0, q_j^r = 0 \end{cases} \quad \forall j \in J, \forall r \in R_j \tag{39}$$

$$Q_j = \sum_r q_j^r, \quad \forall r \in R_j \tag{40}$$

$$x_i = \sum_j \sum_r q_j^r \cdot u_{ijr}, \quad \forall j \in J, \forall r \in R_j \tag{41}$$

$$q_{l,t} = x_i \cdot \beta_i^{l,t}, \quad \forall i \in I \tag{42}$$

Eq. (38) is the additive costs of a path, where u_{ijr} is a 0–1 variable, $u_{ijr} = 1$ if the arc i belongs to path r of OD pair j, otherwise, $u_{ijr} = 0$. Eq. (39) describes the equilibrium condition, i.e., the used paths for an OD have equal and minimum cost and unused paths have costs higher than or equal to the minimum cost. μ_j is the minimum cost of OD j at the UE state, z_j^r is the cost of path r that belongs to OD j, and q_j^r is the passenger flow assigned to path r of OD j. Eq. (40) is the flow conservation on paths, where Q_j is the travel demand of OD j. Eq. (41) gives the passenger volume of arc i. To get the passenger volume $q_{l,t}$ on the track, $\beta_i^{l,t}$ (a 0–1 variable) is introduced in Eq. (42) to represent the passenger volume of arc i, where $\beta_i^{l,t} = 1$ if arc i corresponds to track t on line l, otherwise, $\beta_i^{l,t} = 0$.

In any time instance of the space–time URT network, all expanded arc costs are static and thus the path costs are continuous and non-decreasing with path inflows according to Eqs. (34)–(38). Therefore, given a periodic timetable, a UE state exists after long-term adaptions of path choice (including transfer choices). Existing algorithms such as the Method of Successive Average (MSA) and Routing-Swapping Method are sufficient to find a UE state. The results of the passenger choices at the UE state will be fed to the UL model through Eq. (42) in the bi-level model.

Overall, the proposed optimization framework for generating a periodic energy-efficient timetable relies on assumptions that all passengers can board the train (Assumption 1) and the time-dependent passenger arrival rates at a platform are fixed (Assumption 3) during this period. These assumptions hold in most cases when the passenger demands are evenly distributed in the temporal dimension and not extremely high in the planning period. The model has limitations with uneven and large passenger demands. In that sense, the model framework can be extended by incorporating aperiodic timetables and passenger delays, which however substantially increases the solution space and the difficulty to find a quality solution. As the first endeavor to extend the energy-efficient timetabling from a single line to multiple lines, the bi-level optimization framework divides the decision variables into two parts (i.e., timetable and passenger flow pattens) to cut down the complexity. As it is not straightforward to incorporate the lower-level UE condition as a constraint in the upper-level, we have to resort to a heuristic relaxation process, which cannot guarantee obtaining an optimal solution.

4. Solution algorithm

Bi-level programming is widely applied in transportation research considering two-player interactions (Bracken and McGill, 1973; Yang and Huang, 2004; Gao et al., 2005; Han et al., 2015; Yu et al., 2015; Rashidi et al., 2016; Li and Wan, 2019; Li and Liao, 2020). The bi-level programming for network design problems is proved as an NP-hard (NP: non-deterministic polynomial-time) problem. Several algorithms have been proposed to solve the bi-level model, for example, *meta*-heuristic algorithms and Lagrangian relaxation-based algorithms (Cantarella et al., 2006; Szeto and Jiang, 2014; Liu and Zhou, 2016). As remarked in Section 3.1, given the passenger path choices, we can directly apply an existing solver to obtain the exact solutions. Since the lower level is a static user equilibrium in the space–time network, the method of successive average (MSA) as a proven method is applied. There are usually four steps of the MSA (see the pseudo-code below), including initialization, path generation, traffic impedance updating, and passenger flow assignment (Mounce and Carey, 2015). Although the MSA may get a local optimum, the outer iterations of the upper and lower level models can be utilized to evaluate the quality of a feasible solution.

The pseudo-code of the MSA:

Step 1: Initialization
Set passenger flow vector $\boldsymbol{x}$ as $\mathbf{0}$; calculate traffic impedances for all arcs by Eqs. (34)–(38); set iteration counter $s = 0$.
Step 2: Path generation
Assign passenger demands to the feasible paths generated by the shortest path algorithm with the minimum path impedances; obtain path and arc flows.
Step 3: Update arc impedances
$s = s + 1$; calculate the traffic impedances of all arcs with passenger flow $\boldsymbol{x}^s$.
Step 4: Update the passenger flow assignment
Repeat **Step 2**; obtain new passenger flow $\boldsymbol{y}^s$ and update $\boldsymbol{x}^{s+1} = \boldsymbol{x}^s + (\boldsymbol{y}^s - \boldsymbol{x}^s)/s$.
Step 5: Termination condition
If $s \geq \overline{A}$ or $\|\boldsymbol{x}^{s+1} - \boldsymbol{x}^s\|/\boldsymbol{x}^s \leq \overline{\omega}$, then stop, where $\overline{A}$ and $\overline{\omega}$ are the maximum number of iterations and threshold for convergence respectively; otherwise, $s = s + 1$ and return to **Step 3**.

For the bi-level model, any feasible timetable and passenger path flow together generate an upper bound. To examine the quality of the upper bound, we propose a domain-knowledge based heuristic method to find a lower bound of the optimal energy consumption. Similar to the MSA algorithm performed in the space–time URT network, the MSA algorithm is carried out in a space-energy network to obtain the lower-bound energy consumption. The space-energy network has the same topology as a one-time instance of the space–time network. Link impedances in the space-energy network refer to energy consumption and the energy-related MSA algorithm is called EMSA for short. One major difference is that only running arcs consume energy and the other four types of arcs do not. To obtain a valid lower bound, we use the profile with the minimum energy consumption of an empty train, $e_{l,t}^{0,\min}$, on a running arc. For a further relaxation of the lower bound, we only consider a proportion of the train passengers obtained from the EMSA. It is supposed that the passengers on the space-energy network also reach equilibrium with the lowest energy consumption. Likewise, the impedance of running arcs in the EMSA is updated as

$$c_i = \left(\frac{q_i}{\gamma_l} + \frac{q_i \bullet \tau}{m_l^0}\right) e_{l,t}^{0,\min}, \quad i \in I^r \tag{43}$$

where q_i is the passenger volume on running arc i.

For each line, the frequency is determined the maximum number of passengers on the tracks, $q_l^{\max}$. Therefore, replacing q_i by $q_l^{\max}$ in $\frac{q_i}{\gamma_l}$ of Eq. (43) is closer to the actual frequency. Moreover, as the frequency should be an integer, $\left\lceil \frac{q_l^{\max}}{\gamma_l} \right\rceil$ is the actual frequency with the passenger loading. The impedances of running arcs can be replaced by Eqs. (44)–(45) alternatively to accelerate the passenger flow adjustment and convergence of EMSA.

$$c_i = \left(\frac{q_l^{\max}}{\gamma_l} + \frac{q_i \bullet \tau}{m_l^0}\right) e_{l,t}^{0,\min}, \quad i \in I^r \tag{44}$$

$$c_i = \left(\left\lceil \frac{q_l^{\max}}{\gamma_l} \right\rceil + \frac{q_i \bullet \tau}{m_l^0}\right) e_{l,t}^{0,\min}, \quad i \in I^r \tag{45}$$

Using the minimum energy consumption on each track, a relaxed constraint for the fleet size, and a similar MSA convergence, the EMSA can find a quality approximate lower bound. Integrating the above

modeling components, a solution algorithm to the bi-level model is shown in Fig. 8. Note that, starting from a timetable input, the passenger assignment should be conducted before energy-efficient timetabling. Therefore, the lower level module is swapped to the upside with reference to Fig. 8. The solution algorithm has two stages, in which the "Lower bound" module on the left-hand side aims to find a quality lower bound in Fig. 8(a) and the counterpart on the right-hand side finds a feasible solution for the upper bound in Fig. 8(b). Specifically, at the first stage, we construct the space-energy network S_L and obtain the passenger flow X_L at an imaginative UE state by EMSA; then, we solve the energy-efficient model Eq. (33) to find the lower bound energy consumption E_L and timetable B_L. This stage is completed when a converged E_L is found. Likewise, at the second stage, we construct the space–time network S_U, obtain passenger flow X_U by MSA, and find the minimum energy E_U with feasible timetable B_U. If the relative gap, $\frac{E_U - E_L}{E_U}$, between the upper and lower bounds is not satisfactory, B_U is considered the input to the "Upper bound" module to start the next iteration. The solution algorithm is terminated when a satisfactory relative gap is obtained or the maximum number of iterations is reached.

5. Case study

In this section, we demonstrate the effectiveness of the proposed bi-level model with the URT network in the City of Xi'an (China),

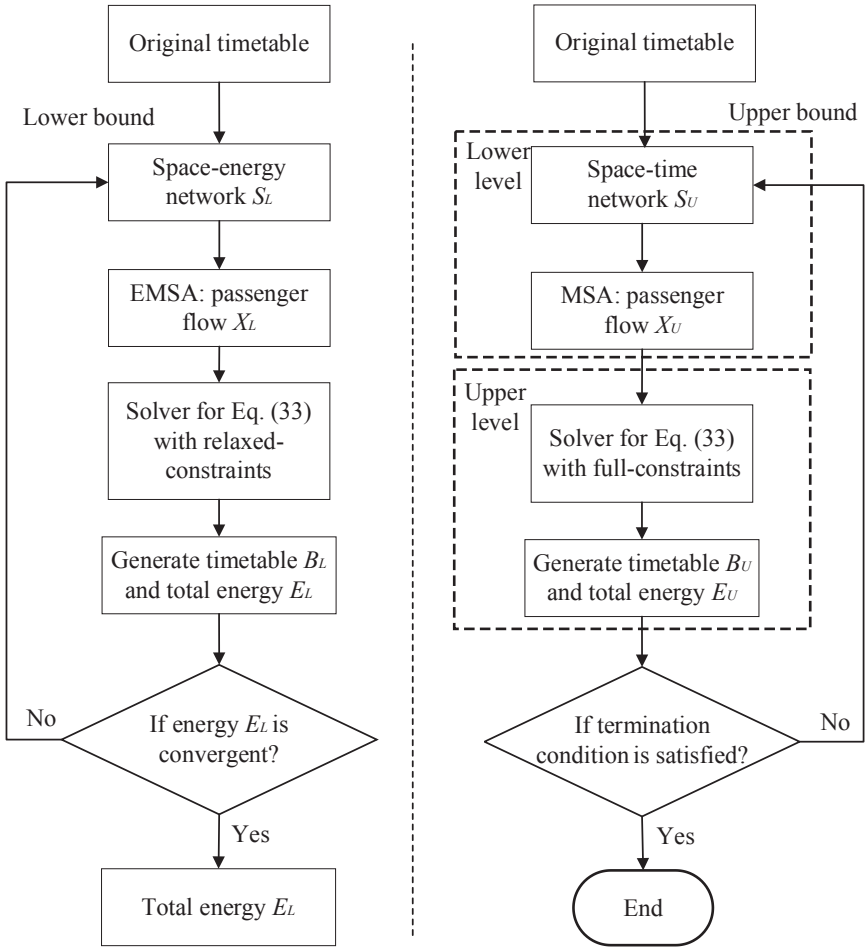

Fig. 8. Solution algorithm flowchart (lower and upper bound are obtained respectively).

which includes 4 lines and 94 stations in service (Fig. 9). Lines 1–4 have 38, 42, 52, and 56 bidirectional platforms respectively. The alternative headways for each line are listed in Table 3. Since a station is extended to three nodes (i.e., two platforms and one virtual node), there are 282 (or 94×3) nodes in a one-time instance of the space–time network. We select a URT operating period between 8:00 am and 9:00 am ($\Gamma = 3600$s) during the morning peak time. The running time and speed profiles for each section are listed in Table A1 (in the Appendix). The model is solved with a personal computer (8G RAM and Intel Core i7-6700U CPU) and Gurobi + python. The parameters in the lower level UE model are set in the unit of disutility/min as, the cost coefficient of waiting time κ^w:1.0, the cost coefficient for crowding of in-vehicle time κ^r: 0.1, cost coefficient range of transfer time κ^t: [1.3, 2.5] (a feasible range suggested by Chen et al. (2015)). The maximum iterations ($\overline{A}$) for MSA and EMSA are set as 500, and $\overline{\omega}$ is set as 10^{-3}. The relative gap threshold, gap_0, is set as 5% for the bi-level model.

To verify the model and algorithm, two cases are presented in an accumulative way. Case 1 shows the effectiveness of the model in the current URT network with a sensitivity test on the key parameter κ^t. To highlight the effects of transfer opportunities in the URT network, Case 2.1 supposes disruptions at the transfer stations; in Case 2.2, we add transfer opportunities from and to new URT lines to be opened to study the influence on energy consumption.

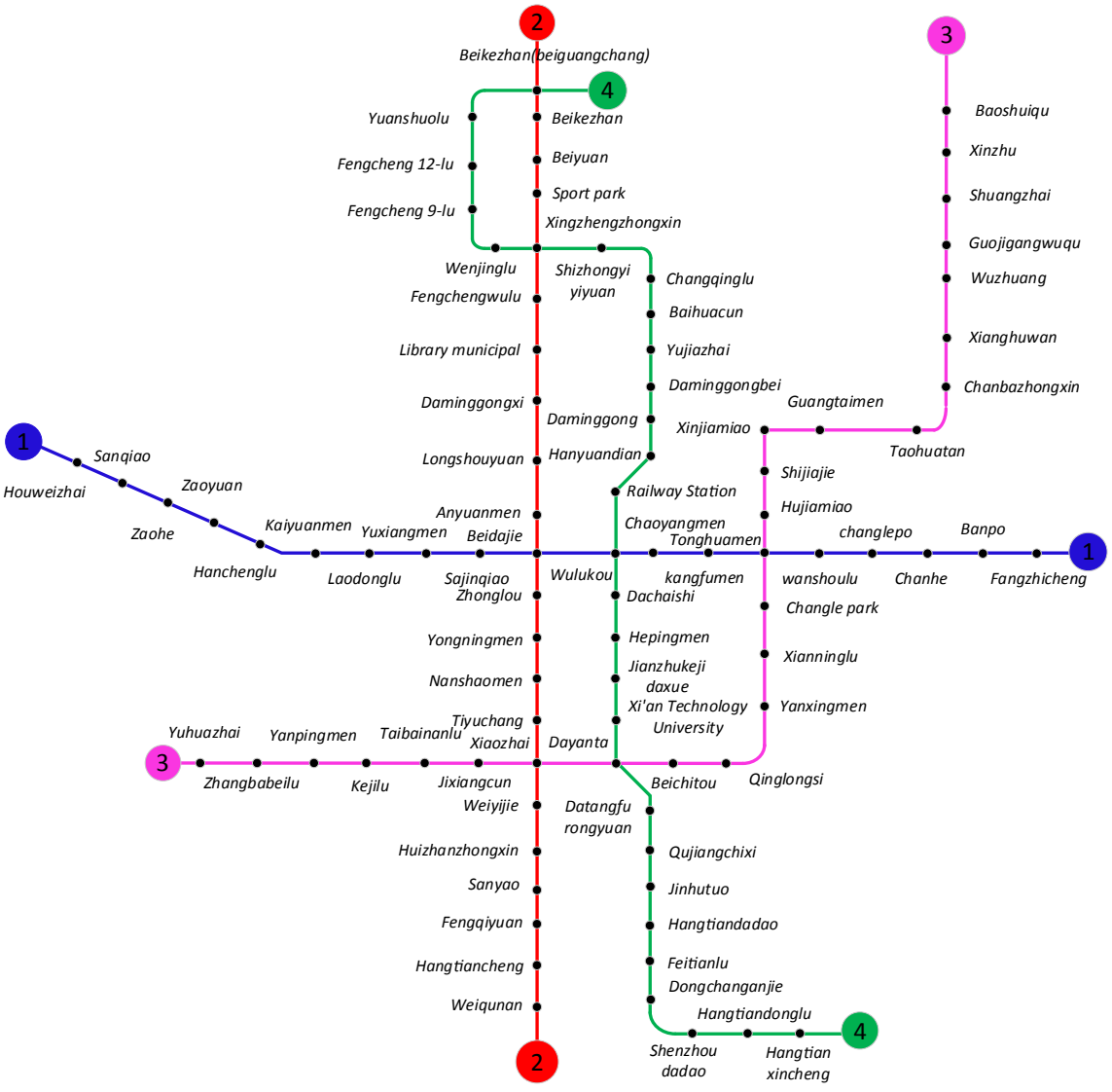

Fig. 9. The Xi'an URT network.

Table 3
The alternative headways for each line.

Line \ headway index	1	2	3	4	5
Line 1	180 s	200 s	240 s	300 s	360 s
Line 2	150 s	180 s	200 s	240 s	300 s
Line 3	150 s	180 s	200 s	240 s	300 s
Line 4	240 s	300 s	360 s	400 s	600 s

5.1. Case 1: URT in the current form

Based on the passenger demand on a weekday, the original timetable consumes energy of 94453.98 kWh, calculated by our model. Considering different values of κ^t and 90% of the train passengers in the lower bound (Section 4), stable timetable solutions are obtained as shown in Fig. 10. Since all upper bounds are stable after ten iterations, the convergent solutions are shown for the first ten outer iterations, which take around 650 s as the average computation time. Taking $\kappa^t = 1.3$ for example, a common setup in MSA (Chen et al., 2015), the upper bound timetable solution consumes energy of 69537.97 kWh as opposed to the lower bound 66807.877 kWh, resulting in a relative gap of 11.97% (or (69537.97–66807.877)/69537.97). Compared with using the current timetable, the solution

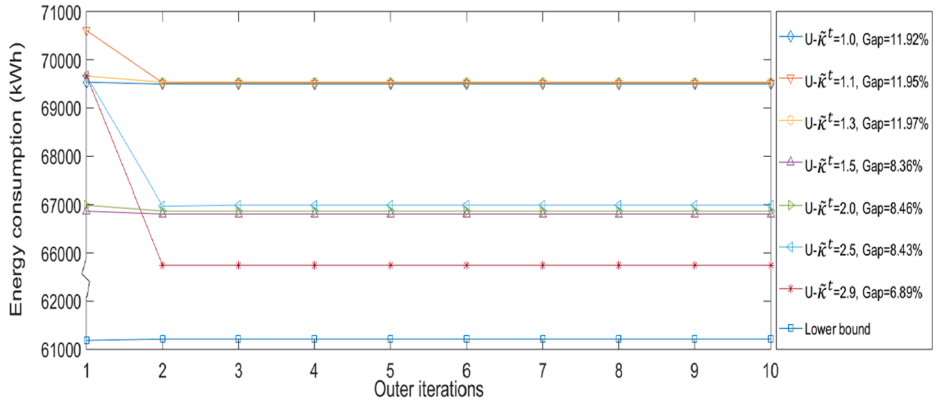

Fig. 10. Results of upper and lower bounds with different κ^t.

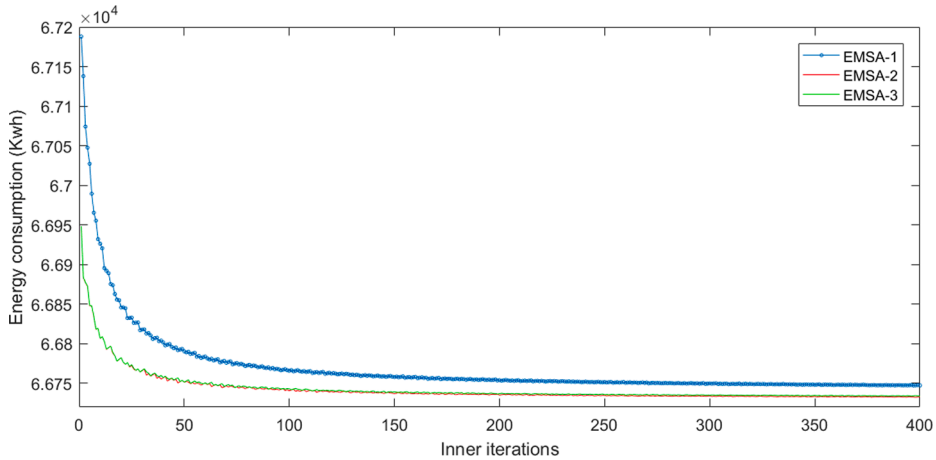

Fig. 11. The convergence of EMSA.

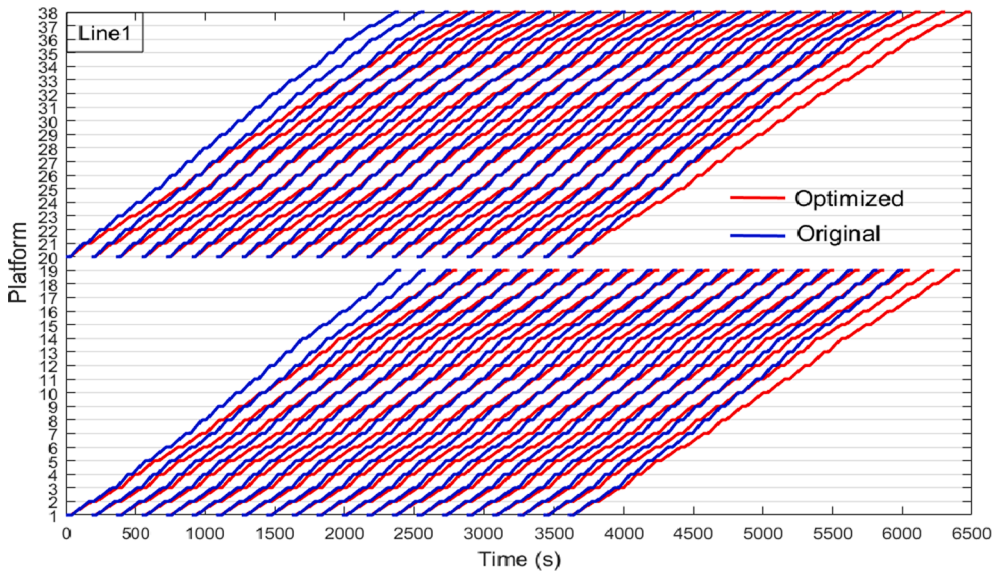

Fig. 12a. The timetable of Line 1.

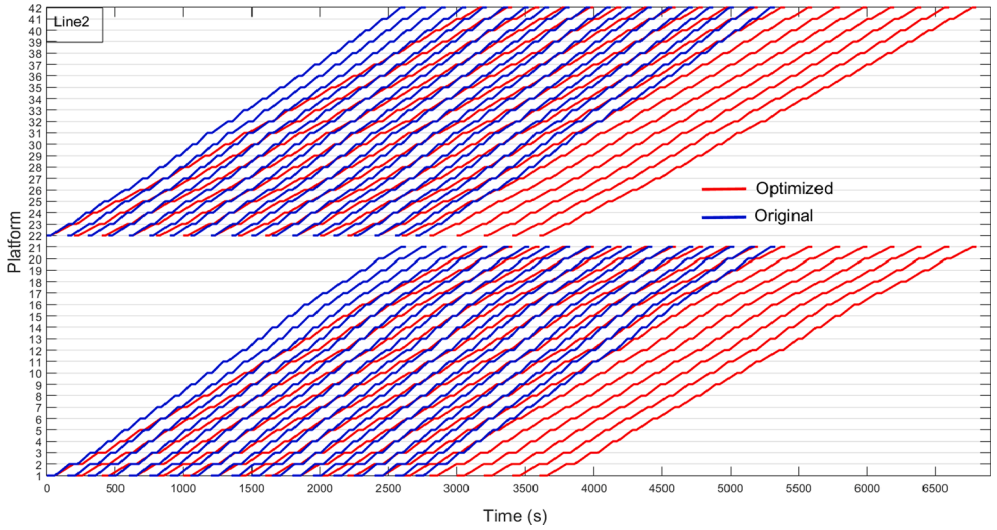

Fig. 12b. The timetable of Line 2.

Fig. 13. Origins and destinations of OD pairs that have different least-cost paths.

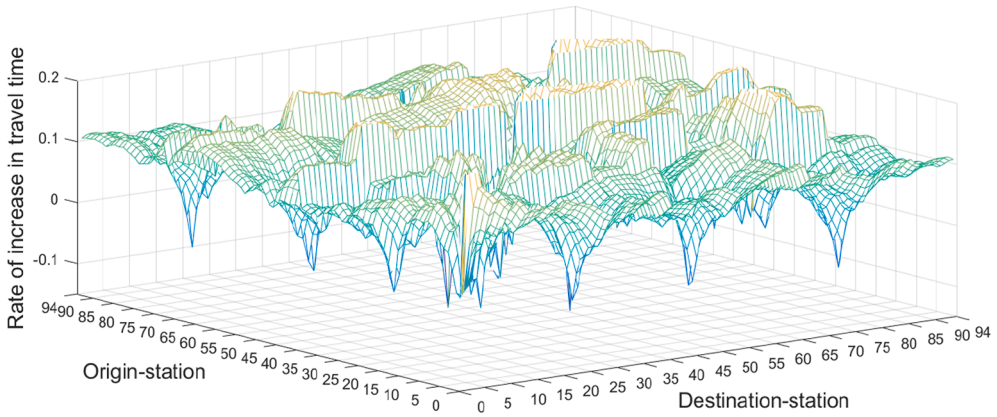

Fig. 14. Change of travel time between every two stations.

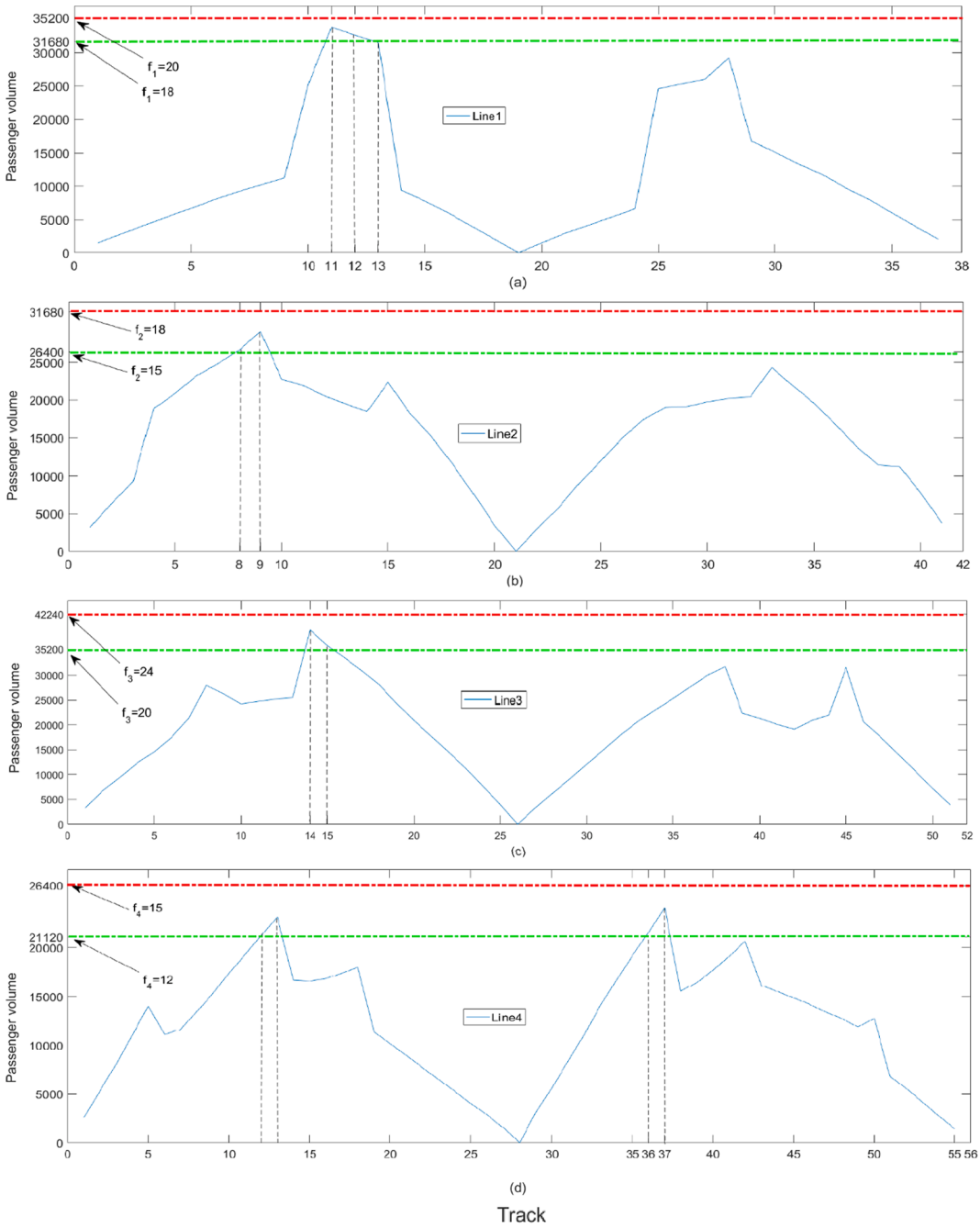

Fig. 15. Passenger volumes on each track of Lines 1–4.

timetable reaches a relative energy reduction by 26.4% (or (94453.98–69537.97)/94453.98). When the κ^t is bigger, it may obtain more energy reduction. For example, $\kappa^t = 1.5$, the relative energy reduction reaches 29.3%. Due to the limited alternatives of train headways (Table 3) and the use of a conservative low bound, the solution space is not large in terms of discrete combinations. We find that the upper bounds are convergent after two iterations and the relative gaps do not reach the pre-specified level with certain specifications of κ^t. The reason is that this example has limited alternatives of train headways (Table 3) and uses a conservative low bound. Comparing the current and optimized timetables, we find that the average proportions of energy consumption caused by passenger weights on all tracks are both around 23%. Although the proportions hardly change after optimization, there is a significant reduction in total energy consumption, implying that timetabling and the passenger assignment process affect energy consumption. Overall, the solution algorithm produces satisfactory timetable solutions based on energy consumption reductions.

The iterative process of EMSA is illustrated in Fig. 11, where EMSA-1, EMSA-2, EMSA-3 correspond to Eqs. (43), (44), and (45) for

updating the impedances of running arcs, respectively. When the iterations get larger, the flow adjustment process is stable and convergent. The results show that Eqs. (44)–(45) (curves in red and green) accelerate the convergence.

The comparisons between the original timetables and optimized timetable (when $\kappa^t = 1.3$) are shown in Figs. 12a–b, in which Lines 1 and 2 are taken for demonstration. In the optimized timetable, all running trains of Line 1 incur a slight delay despite no change in the headway, whereas trains of Line 2 have both slightly increased headway and running times. The results are in line with the basic principles of energy consumption. Specifically, a larger headway means fewer trains on the planning horizon and a delay means a longer running time with lower energy consumption. Therefore, on the condition of transporting all passenger demand, the optimized timetable effectively reduces energy consumption.

To further show which OD pairs may change their paths under the optimized timetable, we record the OD pairs that have different least-cost paths from those under the original timetable. It is found that 896 OD pairs among the total 6588 OD pairs that need transfers have different least-cost paths. The visualization of origins and destinations of those pairs are shown in Fig. 13. The histogram height placed on the stations indicates the number of origins or destinations changing the least-cost path. We can see that the origins and destinations in the city center and northern part are more likely to change their paths under the optimized timetable. The maximum numbers of origins and destinations changing the least-cost path are 33 and 27, which are the Xingzhengzhongxin and Beidajie stations, respectively. This information is useful for aiding the operator to determine if the changes are intended.

A side effect is that passenger travel times may increase unavoidably. However, as shown in Fig. 14, compared with the original timetable, the largest increase of travel time is less than 18% of all OD pairs between the 94 stations of the URT network. It is found that the average travel time of all OD pairs is increased by 9.8% (the average travel time is 34.4 min with the original timetable). All setups being equal, energy-oriented timetabling cannot avoid the expenses of passenger travel time for reducing energy consumption (Chevrier et al., 2013; Yang et al., 2020). However, it appears acceptable to have considerably reduced energy consumption with a slight increase in passenger travel time in an initiative to combat environmental concerns (Mo et al., 2019a). Empirical research is required to achieve an appropriate trade-off between energy consumption and passenger travel time, which is however beyond the scope of this study.

Passenger volumes of Lines 1–4 are displayed in Fig. 15(a)–(d). We find that the passenger volume has two-peaks concentrating on certain tracks near the transfer stations. To transport all passengers with a periodic timetable, the peak volumes determine the frequency of the URT lines. Given that the train mass is much larger than the total passenger weight, a train itself accounts for a significant share of energy consumption. Therefore, a higher frequency means a larger fleet size and higher energy consumption. In Fig. 15(a)–(d), the obtained frequencies are denoted by the red dashed lines. To cut down energy consumption, a slight reduction in the peak volumes can effectively reduce the train frequencies to the green dashed lines, which correspond to the first larger alternative headways than the obtained ones. A larger value of κ^tmakes passengers less concentrate on the track near the transfer stations and results in a lower peak passenger volume. This also explains why a higher value of κ^t leads to a smaller (better) upper bound.

5.2. Case 2.1: Effects of transfer – interrupt of transfer opportunities

To show the effects of transfer between URT lines on the total energy consumption, we deliberately make an interrupt on transfer

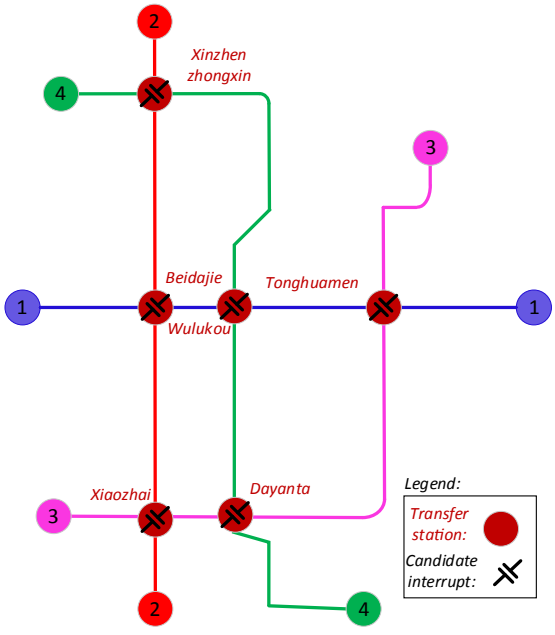

Fig. 16. Interrupt at a transfer station in the Xi'an URT network.

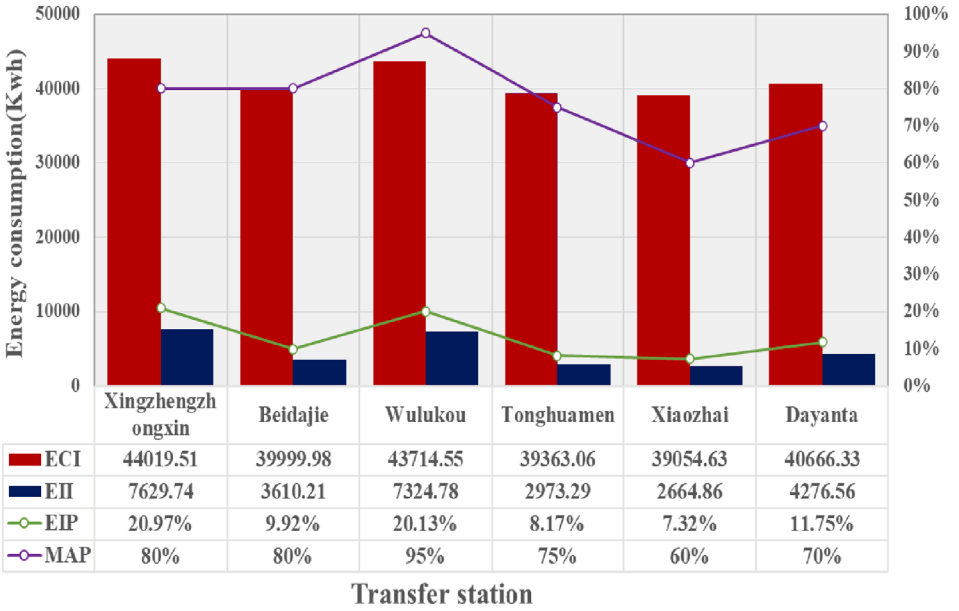

	Xingzhengzhongxin	Beidajie	Wulukou	Tonghuamen	Xiaozhai	Dayanta
ECI	44019.51	39999.98	43714.55	39363.06	39054.63	40666.33
EII	7629.74	3610.21	7324.78	2973.29	2664.86	4276.56
EIP	20.97%	9.92%	20.13%	8.17%	7.32%	11.75%
MAP	80%	80%	95%	75%	60%	70%

Fig. 17. Energy consumption and network vulnerability after the interrupt at a transfer station.

arcs at each transfer station (all transfer directions are interrupted at the station). Note that the interrupts on the transfer arcs at one station do not prevent the URT lines and the other transfer stations from functioning. The setup allows us to evaluate the influence of transfer opportunities due to potential emergencies on a single line separately. First, we consider the original passenger demand as in Case 1. When there is a separate interrupt at each transfer station, as shown in Fig. 16, it is found that the original passenger demand exceeds the capacity of the downgraded URT network and not all passengers can be transported. To show the influence after the interrupt, we define four indicators, "Energy consumption after an interrupt" (ECI), "Energy consumption increase after an interrupt" (EII), "Percentage of energy consumption increase after an interrupt" (EIP), "Maximum allowed percentage of the original passenger demand" (MAP). ECI, EII, and EIP refer to energy consumption change, while MAP reflects the vulnerability of the URT network. The ECI, EII, EIP, and MAP after the interrupt at each transfer station are shown in Fig. 17. It shows that the vulnerabilities of the transfer stations, indicated by MAP, are different. Amongst, the Xiaozhai is the weakest. If the transfer is not allowed, the network cannot even afford 60% of the original passenger demand. The interrupt at Wulukou has the least negative effect (−5%) on the URT network. Since the Wulukou station is located in the central area, the interruption of transfer can be compensated by other transfer stations.

Furthermore, we use 50% of the original passenger demand (less than the values of MAP of all stations) proportionally for all ODs to show the increase in energy consumption. With the reduced demand, the optimal energy consumption is 36389.76 kWh before an interrupt at one of the transfer stations. Based on the indicator of ECI, we find that interrupts significantly increase energy consumption. Particularly, note that the EII and EIP may not change at the same pace with MAP. For example, the interrupts at the Xinzhenzhongxin and Wulukou stations have EII over 7000 kWh, which accounts for EIP about 20%. Interrupts at other stations have also caused about 10% in EIP. However, the Xinzhenzhongxin station has the least vulnerability for transfer, but it has the highest EIP. Combing the above results, from a reversed perspective, we find that transfer stations play an essential role in energy-saving.

5.3. *Case 2.2: Effects of transfer – the addition of transfer opportunities*

To complement Case 2.1, we add transfer arcs based on Case 1 to further verify the influence of transfer opportunities on energy consumption. As shown in Fig. 18, two URT lines (Lines 5 and 6), which will come into operation soon[1], have transfer opportunities with the existing lines at six stations. Since the detailed designs of the newly added URT lines are not available, we use the neighboring parallel sections to approximate the running times and energy consumption. To make interesting comparisons, we also assume that the added transfer opportunities (delineated within the two ellipses) would not introduce new passenger demand. Corresponding to Cases 1 and 2.1, we re-run the model under two scenarios and present the results below.

First, with the original passenger demand in Case 1, the energy consumption after separately adding transfer arcs of Lines 5 and 6 are 67945.27 kWh and 67613.02 kWh, respectively, meaning 2.3% and 2.8% of energy reductions, compared with the optimal solution (69537.97 kWh) in Case 1. When simultaneously adding transfer arcs of Lines 5 and 6, a higher energy reduction of 3.4% (67271.27 kWh) is achieved. Therefore, the transfer and synchronous optimization of multiple lines have a positive reduction in energy consumption.

[1] https://www.xianrail.com/#/planConstruction/linesConstruction.

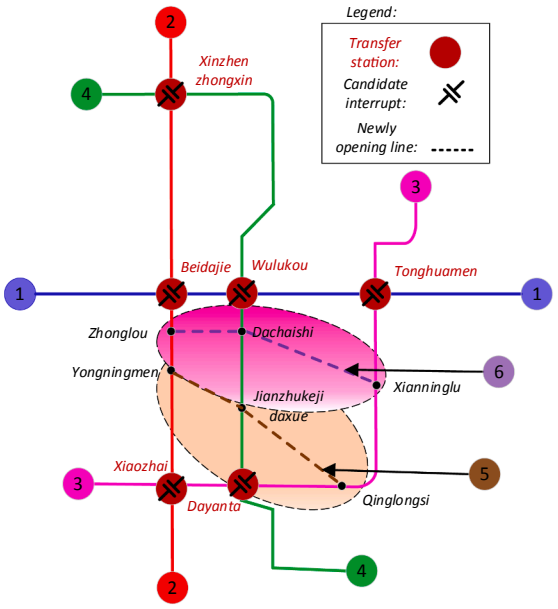

Fig. 18. The transfer arcs of new lines in the Xi'an URT network.

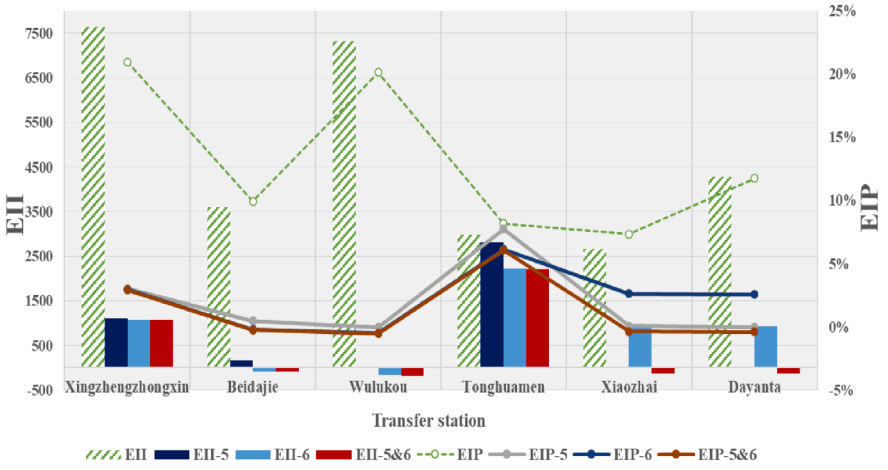

(EII: Energy consumption increase after an interrupt;
EIP: Percentage of energy consumption increase after an interrupt)

Fig. 19. Energy reduction after adding transfer arcs.

Second, considering 50% of the passenger demand in Case 1, we find that the vulnerability and energy consumption after an interrupt at the same station are reduced, compared to Case 2.1. In Fig. 19, '-5′, '-6′, and '-5&6′ are attached to the indicators referring to the addition of transfer arcs with Line 5 only, Line 6 only, and Lines 5–6, respectively. As seen in the histogram, the EII values after the interrupt of transfer opportunities associated with the Beidaijie, Wulikou, Xiaozhai, and Dayanta stations are negative. The EIP values after adding the transfer opportunities show obvious reductions with reference to the green dashed curve (before the addition). Moreover, the vulnerability of the URT network has been reduced after the addition of transfer opportunities, as shown in Fig. 20. The original MAP, denoted by the purple dashed curve, is lower than the solid curves. After adding transfer arcs of Line 5 or Line 6, the MAP values are different due to the interrupt at different stations. Even when the transfer arcs at Beidajie or Wulukou are interrupted, the network can still afford all (100%) of the original passenger demand. When the interrupt happens at Tonghuamen, Xiaozhai, or Danyanta, the maximum affordability of the network is significantly improved after adding the transfer opportunities. Only for the interrupt at the Xinzhengzhongxin station (located in the suburban area), the added transfer opportunities have no effect on the MAP.

Overall, through the above numerical analyses, it can be concluded that the proposed model and the solution algorithm perform well for generating energy-efficient timetables of the URT network with multiple lines. The results also show that the transfer opportunities and passenger path choice significantly influence the total energy consumption of the URT network. For the URT operator,

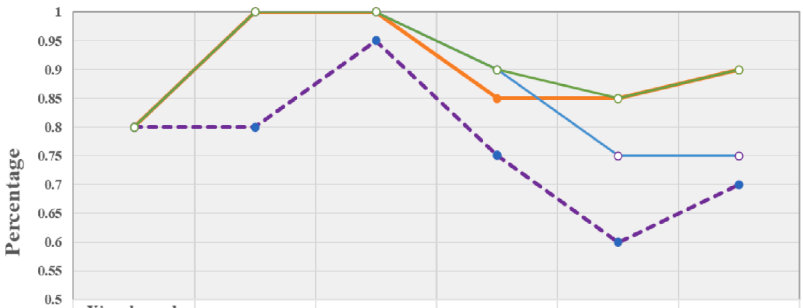

	Xingzhengzhongxin	Beidajie	Wulukou	Tonghuamen	Xiaozhai	Dayanta
MAP	80%	80%	95%	75%	60%	70%
MAP-5	80%	100%	100%	85%	85%	90%
MAP-6	80%	100%	100%	90%	75%	75%
MAP-5&6	80%	100%	100%	90%	85%	90%

Transfer station

(MAP: Original maximum allowed percentage of the original passenger demand.)

Fig. 20. Vulnerability reduction after adding transfer arcs.

the transfer design and control are not only crucial to vulnerability reduction but also important for the energy-saving of the URT network.

6. Conclusions and future work

Existing energy-efficient timetabling has been limited to single URT lines. In the paper, we proposed a bi-level model framework that formulates energy-efficient timetabling of an entire URT network as MILP in the UL and UE-based path choice responding to a timetable in the LL. A heuristics algorithm involving a relaxation process and an MSA module was developed to find near-optimal timetable solutions. The efficiency and effectiveness of the proposed model were demonstrated in experimental examples considering the URT network of Xi'an (China) as a study area. The proposed model can achieve a significant reduction (26.4%) of energy consumption with the compromise of a minor (9.8%) increase in the average travel time compared to the current timetable. To highlight the influence of transfer opportunities and timetable synchronization, sensitivity analyses based on the deletion and addition of transfer arcs are conducted. The results show that transfer opportunities and synchronization between multiple URT lines contribute to saving energy and improving the resilience of the URT network. These results confirm the inaccuracy and insufficiency of the existing energy-efficient timetabling models that ignore the interconnections between multiple URT lines.

Moreover, this study paves the way to several promising research directions. First, the trade-off between energy consumption and passenger travel time should be considered, for which multi-objective energy-efficient timetabling is worth investigation. Second, the solution algorithm should consider space–time networks in the full temporal dimension. In theory, higher resolutions improve the fidelity of the energy-efficient tabling but require more computation resources. Therefore, speedup techniques should be developed for the solution algorithm. Third, some new URT technologies, such as energy regenerative and energy storage devices, could be incorporated into the model framework. Fourth, more realistic passenger path choice behavior should be incorporated in the URT network. Finally, it is important to investigate the relationship between the topology of the URT networks and energy consumption for designing the URT networks. We will address these issues in our future work.

CRediT authorship contribution statement

Kang Huang: Conceptualization, Methodology, Validation, Writing - original draft. **Feixiong Liao:** Conceptualization, Methodology, Writing - review & editing, Supervision. **Ziyou Gao:** Resources, Methodology, Writing - review & editing.

Acknowledgements

This work is jointly supported by the National Natural Science Foundation of China (71621001, 71771018, 71890972/71890970, 71961137001) and the Dutch Research Council (NWO, project no. 438-18-401). The first author is grateful to the financial support by the China Scholarship Council (CSC).

Appendix

See Table A1.

Table A1
The running time and energy consumption of speed profile in three levels.

Platforms	n_1	n_2	n_3	e_1	e_2	e_3	number	Line
Houweizhai_Up	130	141	154	25	21	18	1	Line 1
Sanqiao_Up	132	141	152	24	21.5	17.5	2	Line 1
Zaohe_Up	85	90	95	17	16	15	3	Line 1
Zaoyuan_Up	95	103	112	20	17.5	15	4	Line 1
Hanchenglu_Up	119	134	143	23	19	16	5	Line 1
Kaiyuanmen_Up	112	123	136	23	20	16	6	Line 1
Laodonglu_Up	85	92	100	15	13	11	7	Line 1
Yuxiangmen_Up	91	102	116	18	16	14.5	8	Line 1
Sajinqiao_Up	94	106	120	19	16.5	13.5	9	Line 1
Beidajie_Up	101	110	125	18	15.5	13	10	Line 1
Wulukou_Up	85	97	119	15.5	14	12	11	Line 1
Chaoyangmen_Up	85	92	105	17	15	13	12	Line 1
Kangxialu_Up	85	90	96	14	13	12	13	Line 1
Tonghuamen_Up	116	133	146	23	19	16	14	Line 1
Wanshoulu_Up	110	120	130	23	20	18	15	Line 1
Changlepo_Up	110	122	135	24	20	17	16	Line 1
Chanhe_Up	92	102	123	19	16	14	17	Line 1
Banpo_Up	99	116	132	19	16.5	14	18	Line 1
Fangzhicheng_Up							19	Line 1
Fangzhicheng_Down	95	106	120	19	17	14.5	20	Line 1
Banpo_Down	92	105	126	20	17	15	21	Line 1
Chanhe_Down	98	114	131	20	16.5	14	22	Line 1
Changlepo_Down	104	121	138	19	16	14	23	Line 1
Wanshoulu_Down	103	121	136	19	16.5	14.5	24	Line 1
Tonghuamen_Down	85	90	102	17	15	13	25	Line 1
Kangxialu_Down	84	93	106	17.5	15	13	26	Line 1
Chaoyangmen_Down	89	99	108	18	15.5	13.5	27	Line 1
Wulukou_Down	97	115	129	19	16	14	28	Line 1
Beidajie_Down	91	102	118	18	15.5	14	29	Line 1
Sajinqiao_Down	92	102	117	17	15	13	30	Line 1
Yuxiangmen_Down	93	106	120	18.5	16	13.5	31	Line 1
Laodonglu_Down	103	120	137	20	17	15	32	Line 1
Kaiyuanmen_Down	121	133	145	23	19	16	33	Line 1
Hanchenglu_Down	92	105	119	18	16	14	34	Line 1
Zaoyuan_Down	96	109	124	20	17	14.5	35	Line 1
Zaohe_Down	140	152	163	25	21	18	36	Line 1
Sanqiao_Down	150	165	180	28	25	20	37	Line 1
Houweizhai_Down							38	Line 1
Beikezhan_UP	105	122	138	23	20	18	39	Line 2
Beiyuan_UP	94	106	119	17	15	13	40	Line 2
Yudonggongyuan_Up	90	100	111	17	15	13.5	41	Line 2
Xingzhengzhongxin_Up	89	100	113	17.5	15	13	42	Line 2
Fengchengwulu_Up	92	107	121	19	16	13	43	Line 2
Shitushugaun_Up	93	110	128	16	14	12	44	Line 2
Daminggongxi_Up	99	111	127	19.5	17	14	45	Line 2
Longshouyuan_Up	87	98	111	17.5	15	13	46	Line 2
Anyuanmen_Up	92	111	128	19	16	13	47	Line 2
Beidajie_Up	85	96	108	17	14	12	48	Line 2
Zhonglou_Up	110	128	140	21	18	15	49	Line 2
Yongningmen_Up	82	93	108	17.5	15	13	50	Line 2
Nanshaomen_Up	79	91	104	17	15	13	51	Line 2
Tiyuchang_Up	86	98	111	19	16	13	52	Line 2
Xiaozhai_Up	85	95	108	18	15	12	53	Line 2
Weiyijie_Up	105	120	135	21	18	15	54	Line 2
Huizhanzhongxin_Up	114	136	148	25	20	16	55	Line 2
Sanyao_Up	108	122	139	24	20	16	56	Line 2
Fengqiyuan_Up	100	112	131	22	18	14	57	Line 2
Hangtaincheng_Up	135	144	160	27	23	20	58	Line 2
Weiqunan_Up							59	Line 2
Weiqunan_Down	130	146	160	28	24	20	60	Line 2
Hangtaincheng_Down	97	108	120	20	18	15	61	Line 2
Fengqiyuan_Down	103	118	135	20	18	16	62	Line 2
Sanyao_Down	121	132	151	24	20	16	63	Line 2
Huizhanzhongxin_Down	104	122	137	20	18	16	64	Line 2
Weiyijie_Down	92	107	124	19	16	14	65	Line 2
Xiaozhai_Down	91	105	123	19.5	16	14	66	Line 2
Tiyuchang_Down	89	100	118	18.5	15	13.5	67	Line 2
Nanshaomen_Down	81	95	109	16	14	12	68	Line 2

(*continued on next page*)

Table A1 (*continued*)

Platforms	n_1	n_2	n_3	e_1	e_2	e_3	number	Line
Yongningmen_Down	120	131	148	22	19	16	69	Line 2
Zhonglou_Down	85	96	112	16	14	11	70	Line 2
Beidajie_Down	107	119	132	20	18	12	71	Line 2
Anyuanmen_Down	98	111	128	19	17	14.5	72	Line 2
Longshouyuan_Down	101	113	129	20	18	15	73	Line 2
Daminggongxi_Down	95	109	121	18.5	16	14	74	Line 2
Shitushugaun_Down	96	108	123	18.5	16.5	14	75	Line 2
Fengchengwulu_Down	91	102	119	18	16	13.5	76	Line 2
Xingzhengzhongxin_Down	91	102	119	19	16.5	13	77	Line 2
Yudonggongyuan_Down	96	108	124	19.5	17	14	78	Line 2
Beiyuan_Down	105	121	137	23	20	17.5	79	Line 2
Beikezhan_Down							80	Line 2
Yuhuazhai_Up	141	153	168	28.5	24	20	81	Line 3
Zhangbabeilu_Up	94	107	126	19	17	13.5	82	Line 3
Yanpingmen_Up	105	120	135	20.5	18	14.5	83	Line 3
Kejilu_Up	95	108	125	18.5	16	13.5	84	Line 3
Taibainanlu_Up	100	115	130	20	18	15.5	85	Line 3
Jixiangcun_Up	99	112	131	20	18	15	86	Line 3
Xiaozhai_Up	96	107	120	19.5	17.5	14.5	87	Line 3
Dayanta_Up	93	108	124	19.5	17	14.5	88	Line 3
Beichitou_Up	109	121	138	22	19	16.5	89	Line 3
Qinglongsi_Up	120	133	149	23	20	16.5	90	Line 3
Yanixingmen_Up	72	85	100	17	15	12	91	Line 3
Xianninglu_Up	89	97	110	18	16	13	92	Line 3
Changlegongyuan_Up	80	94	108	18.5	16	13	93	Line 3
Tonghuamen_Up	78	89	103	17	15.5	12	94	Line 3
Hujiamiao_Up	106	118	135	19.5	18	15.5	95	Line 3
Shijiajie_Up	98	110	127	20	18	15	96	Line 3
Xinjiamiao_Up	124	136	151	26	22	19	97	Line 3
Guangtaimen_Up	112	126	140	23	19	17	98	Line 3
Taohautan_Up	100	115	130	21	18	16	99	Line 3
Chanbazhongxin_Up	99	112	130	20.5	18.5	16	100	Line 3
Xianghuwan_Up	124	139	153	27.5	22	18.5	101	Line 3
Wuzhaung_Up	140	150	160	26.5	23	20.5	102	Line 3
Guojigangwuqu_Up	94	108	123	19	17	13.5	103	Line 3
Shaungzhai_Up	92	107	122	19.5	17.5	14	104	Line 3
Xinzhu_Up	92	102	117	19	16.5	13.5	105	Line 3
Baoshuiqu_Up							106	Line 3
Baoshuiqu_Down	90	102	114	19	17.5	15	107	Line 3
Xinzhu_Down	92	105	118	19	17	15	108	Line 3
Shaungzhai_Down	94	108	121	19.5	17	14.5	109	Line 3
Guojigangwuqu_Down	135	150	165	28	24	21	110	Line 3
Wuzhaung_Down	121	139	154	24	21	19	111	Line 3
Xianghuwan_Down	98	112	127	20.5	18.5	16	112	Line 3
Chanbazhongxin_Down	97	115	132	21	18.5	16.5	113	Line 3
Taohautan_Down	110	126	141	21	19	16.5	114	Line 3
Guangtaimen_Down	120	136	152	27	22	19	115	Line 3
Xinjiamiao_Down	97	110	126	19.5	17	15.5	116	Line 3
Shijiajie_Down	93	106	121	19	17	15.5	117	Line 3
Hujiamiao_Down	78	94	110	17.5	16	14.5	118	Line 3
Tonghuamen_Down	80	96	111	17.5	16	15	119	Line 3
Changlegongyuan_Down	89	99	114	18	16	14.5	120	Line 3
Xianninglu_Down	72	89	103	19	16.5	14	121	Line 3
Yanixingmen_Down	121	133	150	24.5	21	18	122	Line 3
Qinglongsi_Down	121	134	145	24	21	18.5	123	Line 3
Beichitou_Down	108	119	134	22	19	15.5	124	Line 3
Dayanta_Down	107	121	138	23	20	16	125	Line 3
Xiaozhai_Down	99	113	129	20	18	15	126	Line 3
Jixiangcun_Down	115	130	145	24	21	19	127	Line 3
Taibainanlu_Down	95	110	125	20	18	16	128	Line 3
Kejilu_Down	105	120	135	24	21	17	129	Line 3
Yanpingmen_Down	94	110	126	22	20	17	130	Line 3
Zhangbabeilu_Down	140	153	168	27.5	23	19	131	Line 3
Yuhuazhai_Down							132	Line 3
Beikezhanbeiguangchang_Up	155	170	186	30	25	21	133	Line 4
Yuanshuolu_Up	85	98	113	17	15	12	134	Line 4
Fengcheng12lu_Up	102	117	132	18	16	13.5	135	Line 4
Fengcheng9lu_Up	103	118	135	20	18	15.5	136	Line 4
Wenjinglu_Up	95	101	117	20	18	15.5	137	Line 4

(*continued on next page*)

Table A1 (*continued*)

Platforms	n_1	n_2	n_3	e_1	e_2	e_3	number	Line
Xingzhengzhongxin_Up	112	127	139	22	20	18	138	Line 4
Shizhongyiyiyuan_Up	122	136	153	26	23	19	139	Line 4
Changqinglu_Up	102	116	132	21	19	16	140	Line 4
Baihuacun_Up	106	120	137	21.5	18	16	141	Line 4
Yujiazhai_Up	108	121	140	21	18.5	15.5	142	Line 4
Daminggongbei_Up	120	134	150	24	20	17	143	Line 4
Daminggong_Up	99	115	130	20	18	15.5	144	Line 4
Hanyuandian_Up	190	210	230	31	28	25	145	Line 4
Wulukou_Up	108	121	137	20.5	18.5	16	146	Line 4
Dachaishi_Up	102	116	132	20	17.5	15.5	147	Line 4
Hepingmen_Up	102	117	135	20	17.5	15	148	Line 4
Jianzhudaxue_Up	92	108	123	18.5	16.5	14.5	149	Line 4
Xiankejidaxue_Up	102	116	130	19	17	14.5	150	Line 4
Dayanta_Up	169	185	200	28	24	21	151	Line 4
Datangfurongyuan_Up	155	160	175	27	22	20	152	Line 4
Qujiangchixi_Up	175	190	205	29	25	22	153	Line 4
Jinhutuo_Up	120	135	150	23	20	18	154	Line 4
Hangtiandadao_Up	95	110	125	20.5	18.5	16	155	Line 4
Feitianlu_Up	110	125	140	20.5	17.5	15	156	Line 4
Dongchanganjie_Up	175	190	213	29.5	25	21	157	Line 4
Shengzhoudadao_Up	105	120	136	20	17.5	15	158	Line 4
Hangtiandonglu_Up	154	170	185	27	23	20	159	Line 4
Hangtianxincheng_Up							160	Line 4
Hangtianxincheng_Down	138	152	170	25	22	19	161	Line 4
Hangtiandonglu_Down	120	135	150	23	20	18	162	Line 4
Shengzhoudadao_Down	180	195	213	28.5	25	22	163	Line 4
Dongchanganjie_Down	112	130	145	22	19	17	164	Line 4
Feitianlu_Down	93	100	115	17.5	16	14	165	Line 4
Hangtiandadao_Down	105	120	135	20	17.5	15	166	Line 4
Jinhutuo_Down	176	190	205	30	26	21	167	Line 4
Qujiangchixi_Down	145	160	175	26	22	19	168	Line 4
Datangfurongyuan_Down	170	185	200	25.5	23	20	169	Line 4
Dayanta_Down	102	117	135	20	17.5	15.5	170	Line 4
Xiankejidaxue_Down	92	107	125	19	17	15	171	Line 4
Jianzhudaxue_Down	102	117	135	20	17	15	172	Line 4
Hepingmen_Down	116	132	150	22	19	17	173	Line 4
Dachaishi_Down	121	137	155	23	20	18	174	Line 4
Wulukou_Down	195	210	225	29.5	24	20	175	Line 4
Hanyuandian_Down	99	116	132	18.5	16.5	14	176	Line 4
Daminggong_Down	134	151	168	22	19	16	177	Line 4
Daminggongbei_Down	108	124	138	19.5	17.5	15.5	178	Line 4
Yujiazhai_Down	106	121	137	19.5	17	15	179	Line 4
Baihuacun_Down	102	119	135	20	17.5	15.5	180	Line 4
Changqinglu_Down	122	136	153	26	22.5	20	181	Line 4
Shizhongyiyiyuan_Down	112	127	145	23.5	20	18.5	182	Line 4
Xingzhengzhongxin_Down	95	110	125	18.5	16.5	15	183	Line 4
Wenjinglu_Down	103	116	134	20	17.5	15	184	Line 4
Fengcheng9lu_Down	102	118	135	18.5	16.5	14	185	Line 4
Fengcheng12lu_Down	85	100	115	18	15.5	13	186	Line 4
Yuanshuolu_Down	160	175	190	28.5	23.5	20	187	Line 4
Beikezhanbeiguangchang_Down							188	Line 4

References

Albrecht, A.R., Howlett, P.G., Pudney, P.J., Vu, X., 2013. Energy-efficient train control: from local convexity to global optimization and uniqueness. Automatica 49, 3072–3078.

Albrecht, A., Howlett, P., Pudney, P., Vu, X., Zhou, P., 2016a. The key principles of optimal train control—Part 1: Formulation of the model, strategies of optimal type, evolutionary lines, location of optimal switching points. Transp. Res. Part B 94, 482–508.

Albrecht, A., Howlett, P., Pudney, P., Vu, X., Zhou, P., 2016b. The key principles of optimal train control—Part 2: Existence of an optimal strategy, the local energy minimization principle, uniqueness, computational techniques. Transp. Res. Part B 94, 509–538.

Bie, J., Lo, H.K., 2010. Stability and attraction domains of traffic equilibria in a day-to-day dynamical system formulation. Transp. Res. Part B 44 (1), 90–107.

Boroun, M., Ramezani, S., Vasheghani Farahani, N., Hassannayebi, E., Abolmaali, S., Shakibayifar, M., 2020. An efficient heuristic method for joint optimization of train scheduling and stop planning on double-track railway systems. INFOR: Inform. Syst. Operat. Res. 58 (4), 652–679.

Bracken, J., McGill, J.T., 1973. Mathematical programs with optimization problems in the constraints. Operat. Res. 21 (1), 37–44.

Cai, X., Goh, C.J., 1994. A fast heuristic for the train scheduling problem. Comput. Oper. Res. 21 (5), 499–510.

Canca, D., Zarzo, A., 2017. Design of energy-efficient timetables in two-way railway rapid transit lines. Transp. Res. Part B 102, 142–161.

Cantarella, G.E., Pavone, G., Vitetta, A., 2006. Heuristics for urban road network design: lane layout and signal settings. Eur. J. Oper. Res. 175 (3), 1682–1695.

Ceder, A., Tal, O., 2001. Designing synchronization into bus timetables. Transport. Res. Rec.: J. Transport. Res. Board 1760 (1), 28–33.

Chen, B., Si, B., Jiang, M., Yang, X., 2015. Scheduled- based equilibrium assignment model and algorithm for urban subway network. Sci. China: Technol. Sci. 45 (12), 1269–1278.
Chen, Y., Mao, B., Bai, Y., Ho, T.K., Li, Z., 2019. Timetable synchronization of last trains for urban rail networks with maximum accessibility. Transp. Res. Part C 99, 110–129.
Chevrier, R., Pellegrini, P., Rodriguez, J., 2013. Energy saving in railway timetabling: A bi-objective evolutionary approach for computing alternative running times. Transp. Res. Part C 37, 20–41.
Djavadian, S., Chow, J.Y., 2017. Agent-based day-to-day adjustment process to evaluate dynamic flexible transport service policies. Transportmetrica B: Transp. Dyn. 5 (3), 281–306.
Fu, X., Lam, W.H., 2018. Modelling joint activity-travel pattern scheduling problem in multi-modal transit networks. Transportation 45 (1), 23–49.
Gao, Z., Wu, J., Sun, H., 2005. Solution algorithm for the bi-level discrete network design problem. Transp. Res. Part B 39 (6), 479–495.
Gentile, G., Nguyen, S., Pallottino, S., 2005. Route choice on transit networks with online information at stops. Transport. Sci. 39 (3), 289–297.
González-Gil, A., Palacin, R., Batty, P., 2013. Sustainable urban rail systems: Strategies and technologies for optimal management of regenerative braking energy. Energy Convers. Manage. 75, 374–388.
González-Gil, A., Palacin, R., Batty, P., Powell, J.P., 2014. A systems approach to reduce urban rail energy consumption. Energy Convers. Manage. 80, 509–524.
Guo, X., Wu, J., Zhou, J., Yang, X., Wu, D., Gao, Z., 2018. First-train timing synchronisation using multi-objective optimisation in urban transit networks. Int. J. Prod. Res. 57 (11), 3522–3537.
Guo, X., Wu, J., Sun, H., Yang, X., Jin, J., Wang, Z., 2020. Scheduling synchronization in urban rail transit networks: Trade-offs between transfer passenger and last train operation. Transp. Res. Part A 138, 463–490.
Gupta, S.D., Tobin, J.K., Pavel, L., 2016. A two-step linear programming model for energy-efficient timetables in metro railway networks. Transp. Res. Part B 93, 57–74.
Han, K., Sun, Y., Liu, H., Friesz, T.L., Yao, T., 2015. A bi-level model of dynamic traffic signal control with continuum approximation. Transp. Res. Part C 55, 409–431.
Howlett, P., Pudney, P., 1995. Energy-Efficient Train Control. Advances in Industrial Control. Springer, London.
Howlett, P., 1996. Optimal strategies for the control of a train. Automatica 32 (4), 519–532.
Howlett, P., Pudney, P., 1998. An optimal driving strategy for a solar powered car on an undulating road. Dyn. Cont. Discrete Impulsive Syst. 4, 553–567.
Howlett, P., 2000. The optimal control of a train. Ann. Oper. Res. 98, 65–87.
Howlett, P., Pudney, P., Vu, X., 2009. Local energy minimization in optimal train control. Automatica 45 (11), 2692–2698.
Huang, K., Wu, J., Yang, X., Gao, Z., Liu, F., Zhu, Y., 2019. Discrete train speed profile optimization for urban rail transit: A data-driven model and integrated algorithms based on machine learning. J. Adv. Transport. 4, 1–17.
Huang, K., Wu, J., Liao, F., Sun, H., He, F., Gao, Z., 2021. Incorporating multimodal coordination into timetabling optimization of the last trains in an urban railway network. Transp. Res. Part C 124, 102889.
Jiang, Y., Szeto, W.Y., 2016. Reliability-based stochastic transit assignment: Formulations and capacity paradox. Transp. Res. Part B 93, 181–206.
Khmelnitsky, E., 2000. On an optimal control problem of train operation. IEEE Trans. Autom. Control 45 (7), 1257–1266.
Lai, Q., Liu, J., Haghani, A., Meng, L., Wang, Y., 2020. Energy-efficient speed profile optimization for medium-speed maglev trains. Transp. Res. Part E 102007.
Li, Q., Liao, F., 2020. Incorporating vehicle self-relocations and traveler activity chains in a bi-level model of optimal deployment of shared autonomous vehicles. Transp. Res. Part B 140, 151–175.
Li, T., Wan, Y., 2019. Estimating the geographic distribution of originating air travel demand using a bi-level optimization model. Transp. Res. Part E 131, 267–291.
Li, X., Lo, H.K., 2014a. An energy-efficient scheduling and speed control approach for metro rail operations. Transp. Res. Part B 64, 73–89.
Li, X., Lo, H.K., 2014b. Energy minimization in dynamic train scheduling and control for metro rail operations. Transp. Res. Part B 70, 269–284.
Liu, P., Liao, F., Huang, H.J., Timmermans, H., 2016. Dynamic activity-travel assignment in multi-state supernetworks under transport and location capacity constraints. Transportmetrica A 12 (7), 572–590.
Liu, P., Yang, L., Gao, Z., Huang, Y., Li, S., Gao, Y., 2018. Energy-efficient train timetable optimization in the subway system with energy storage devices. IEEE Trans. Intell. Transp. Syst. 19 (12), 3947–3963.
Liu, P., Schmidt, M., Kong, Q., Wagenaar, J.C., Yang, L., Gao, Z., Zhou, H., 2020. A robust and energy-efficient train timetable for the subway system. Transp. Res. Part C 121, 102822.
Liu, R., Golovitcher, I., 2003. Energy-efficient operation of rail vehicles. Transp. Res. Part A 37, 917–932.
Liu, J., Zhou, X., 2016. Capacitated transit service network design with boundedly rational agents. Transp. Res. Part B 93, 225–250.
Lv, H., Zhang, Y., Huang, K., Yu, X., Wu, J., 2019. An energy-efficient timetable optimization approach in a bi-direction urban rail transit line: a mixed-integer linear programming model. Energies 12 (14), 2686.
Mo, P., Yang, L., Wang, Y., Qi, J., 2019a. A flexible metro train scheduling approach to minimize energy cost and passenger waiting time. Comput. Ind. Eng. 132, 412–432.
Mo, P., Yang, L., D'Ariano, A., Yin, J., Yao, Y., Gao, Z., 2019b. Energy-efficient train scheduling and rolling stock circulation planning in a metro line: a linear programming approach. IEEE Trans. Intell. Transp. Syst. 21 (9), 3621–3633.
Mounce, R., Carey, M., 2015. On the convergence of the method of successive averages for calculating equilibrium in traffic networks. Transport. Sci. 49 (3), 535–542.
Nguyen, S., Pallottino, S., 1988. Equilibrium traffic assignment for large scale transit networks. Eur. J. Oper. Res. 37 (2), 176–186.
Nuzzolo, A., Russo, F., Crisalli, U., 2001. A doubly dynamic schedule-based assignment model for transit networks. Transport. Sci. 35 (3), 268–285.
Panou, K., Tzieropoulos, P., Emery, D., 2013. Railway driver advice systems: Evaluation of methods, tools and systems. J. Rail Transp. Plann. Manage. 3 (4), 150–162.
Qu, Y., Wang, H., Wu, J., Yang, X., Yin, H., Zhou, L., 2020. Robust optimization of train timetable and energy efficiency in urban rail transit: a two-stage approach. Comput. Ind. Eng. 146, 106594.
Rashidi, E., Parsafard, M., Medal, H., Li, X., 2016. Optimal traffic calming: A mixed-integer bi-level programming model for locating sidewalks and crosswalks in a multimodal transportation network to maximize pedestrians' safety and network usability. Transp. Res. Part E 91, 33–50.
Scheepmaker, G.M., Goverde, R.M., Kroon, L.G., 2017. Review of energy-efficient train control and timetabling. Eur. J. Oper. Res. 257 (2), 355–376.
Shang, P., Li, R., Liu, Z., Yang, L., Wang, Y., 2018. Equity-oriented skip-stopping schedule optimization in an oversaturated urban rail transit network. Transp. Res. Part C 89, 321–343.
Shang, P., Li, R., Guo, J., Xian, K., Zhou, X., 2019. Integrating Lagrangian and Eulerian observations for passenger flow state estimation in an urban rail transit network: a space-time-state hyper network-based assignment approach. Transp. Res. Part B 121, 135–167.
Spiess, H., Florian, M., 1989. Optimal strategies: a new assignment model for transit networks. Transp. Res. Part B 23 (2), 83–102.
Su, S., Wang, X., Cao, Y., Yin, J., 2019. An Energy-Efficient Train Operation Approach by Integrating the Metro Timetabling and Eco-Driving. IEEE Trans. Intell. Transp. Syst. https://doi.org/10.1109/TITS.2019.2939358.
Sun, H., Wu, J., Ma, H., Yang, X., Gao, Z., 2018. A bi-objective timetable optimization model for urban rail transit based on the time-dependent passenger volume. IEEE Trans. Intell. Transp. Syst. 20 (2), 604–615.
Szeto, W.Y., Jiang, Y., 2014. Transit route and frequency design: Bi-level modeling and hybrid artificial bee colony algorithm approach. Transp. Res. Part B 67, 235–263.
Wang, P., Goverde, R.M., 2016. Multiple-phase train trajectory optimization with signalling and operational constraints. Transp. Res. Part C 69, 255–275.
Wang, P., Goverde, R.M., 2017. Multi-train trajectory optimization for energy efficiency and delay recovery on single-track railway lines. Transp. Res. Part B 105, 340–361.
Wang, P., Goverde, R.M., 2019. Multi-train trajectory optimization for energy-efficient timetabling. Eur. J. Oper. Res. 272 (2), 621–635.
Wardrop, J.G.,1952. Some theoretical aspects of road traffic research. ICE Proceedings: Engineering Divisions.
Wong, R.C., Yuen, T.W., Fung, K.W., Leung, J.M., 2008. Optimizing timetable synchronization for rail mass transit. Transport. Sci. 42 (1), 57–69.
Wu, J.H., Florian, M., Marcotte, P., 1994. Transit equilibrium assignment: a model and solution algorithms. Transport. Sci. 28 (3), 193–203.

Yang, H., Huang, H.J., 2004. The multi-class, multi-criteria traffic network equilibrium and systems optimum problem. Transp. Res. Part B 38 (1), 1–15.
Yang, S., Wu, J., Sun, H., Yang, X., Gao, Z., Chen, A., 2018. Bi-objective non-linear programming with minimum energy consumption and passenger waiting time for metro systems, based on the real-world smart-card data. Transportmetrica B 6 (4), 302–319.
Yang, S., Wu, J., Yang, X., Liao, F., Li, D., Wei, Y., 2019. Analysis of energy consumption reduction in metro systems using rolling stop-skipping patterns. Comput. Ind. Eng. 127, 129–142.
Yang, S., Liao, F., Wu, J., Timmermans, H.J., Sun, H., Gao, Z., 2020. A bi-objective timetable optimization model incorporating energy allocation and passenger assignment in an energy-regenerative metro system. Transp. Res. Part B 133, 85–113.
Yang, X., Chen, A., Li, X., Ning, B., Tang, T., 2015. An energy-efficient scheduling approach to improve the utilization of regenerative energy for metro systems. Transp. Res. Part C 57, 13–29.
Yang, X., Chen, A., Ning, B., Tang, T., 2016. A stochastic model for the integrated optimization on metro timetable and speed profile with uncertain train mass. Transp. Res. Part B 91, 424–445.
Yang, X., Chen, A., Ning, B., Tang, T., 2017. Bi-objective programming approach for solving the metro timetable optimization problem with dwell time uncertainty. Transp. Res. Part E 22–37.
Yao, Y., Zhu, X., Shi, H., Shang, P., 2019. Last train timetable optimization considering detour routing strategy in an urban rail transit network. Measur. Control 52 (9–10), 1461–1479.
Ye, H., Liu, R., 2016. A multiphase optimal control method for multi-train control and scheduling on railway lines. Transp. Res. Part B 93, 377–393.
Yin, J., Tang, T., Yang, L., Gao, Z., Ran, B., 2016. Energy-efficient metro train rescheduling with uncertain time-variant passenger demands: An approximate dynamic programming approach. Transp. Res. Part B 91, 178–210.
Yin, J., Yang, L., Tang, T., Gao, Z., Ran, B., 2017. Dynamic passenger demand oriented metro train scheduling with energy-efficiency and waiting time minimization: Mixed-integer linear programming approaches. Transp. Res. Part B 97, 182–213.
Yin, J., Su, S., Xun, J., Tang, T., Liu, R., 2020. Data-driven approaches for modeling train control models: comparison and case studies. ISA Trans. 98, 349–363.
Yu, B., Kong, L., Sun, Y., Yao, B., Gao, Z., 2015. A bi-level programming for bus lane network design. Transp. Res. Part C 55, 310–327.
Zhang, Y., Peng, Q., Yao, Y., Zhang, X., Zhou, X., 2019. Solving cyclic train timetabling problem through model reformulation: extended time-space network construct and alternating direction method of multipliers methods. Transp. Res. Part B 128, 344–379.
Zhao, N., Roberts, C., Hillmansen, S., Nicholson, G., 2015. A multiple train trajectory optimization to minimize energy consumption and delay. IEEE Trans. Intell. Transp. Syst. 16 (5), 2363–2372.
Zhong, Q., Lusby, R.M., Larsen, J., Zhang, Y., Peng, Q., 2019. Rolling stock scheduling with maintenance requirements at the Chinese High-Speed Railway. Transp. Res. Part B 126, 24–44.
Zhong, Q., Zhang, Y., Wang, D., Zhong, Q., Wen, C., Peng, Q., 2020. A mixed integer linear programming model for rolling stock deadhead routing before the operation period in an urban rail transit line. J. Adv. Transport. 2020.